

A Scenario Based Fire Susceptibility Approach for Remote Sensing Platform Comparison: Los Angeles County Area, Southern California, USA

by

Nemanja Bisenic

A Thesis Presented to the  
FACULTY OF THE USC DORNSIFE, COLLEGE OF LETTERS, ARTS AND SCIENCES  
University of Southern California  
In Partial Fulfillment of the  
Requirements for the Degree  
Master of Science  
(Geographic Information Science and Technology)

August 2022

## **Dedication**

To my family, thank you for encouraging my desire to learn new things.

## **Acknowledgements**

I am grateful to my mentor, Professor Fleming , for the direction I needed and Professor Ruddell and Professor Sedano who gave me assistance when I needed it. I would like to thank my employer, LAUSD, who allowed me to complete some of this work. I am grateful for the data provided to me by Planet, NASA, and USGS Organizations and the assistance in coding the analysis given my friend, Goran Gogic.

## Table of Contents

Dedication.....	ii
Acknowledgements.....	iii
List of Tables .....	vii
List of Figures.....	viii
List of Abbreviations .....	x
Abstract.....	xi
Chapter 1 Introduction .....	1
1.1. Study Objective.....	2
1.2. Motivation.....	3
1.2.1. Fire health Hazard.....	3
1.2.2. Fire Advisory .....	5
1.3. Study Area .....	6
Chapter 2 Literature Review.....	8
2.1. Regional Context .....	8
2.1.1. Multidimensional Data.....	9
2.1.2. Pre-Fire Indices.....	10
2.1.3. Data Transformation .....	12
2.2. Relevant Studies for Weighted Pre-Fire Susceptibility Scenario .....	12
2.2.1. Angeles National Forest Site Selection for Fire Susceptibility Scenario Using Planet and DEM Data.....	13
2.2.2. Adding DEM Data .....	14
2.3. Scale and Resolution Problem .....	15
2.3.1. Tradeoff Between Resolutions.....	16
Chapter 3 – A Scenario Based Evaluation Framework for Fire Hazard Assessment.....	18

3.1. Data Sources .....	18
3.2. Regional Analysis with IDRISI Terr-Set .....	20
3.2.1. NMDI and NDWI Analysis .....	21
3.2.2. Principal Component Analysis -PCA .....	22
3.3. Raster Predictive Scenario .....	23
3.3.1. Creating Mosaic Datasets .....	23
3.4. Weighted Fire Susceptibility Scenario with Planet-Scope Imagery, DEM derivatives, Electric Lines, and TIGER/Roads Shapefile .....	27
3.4.1. Distance Accumulation .....	27
3.4.2. Electric Lines .....	29
3.4.3. DEM Layer Processing .....	30
3.4.4. Creating Hill-shade and Slope Layers .....	31
3.4.5. NDVI Layer from PlanetScope Data .....	32
3.4.6. Susceptibility Synthesis .....	33
Chapter 4 Regional and Local Results .....	35
4.1. Raster Predictive Scenario .....	35
4.1.1. Temporal Profile .....	36
4.1.2. Trend .....	40
4.1.3. Raster Predictive Model .....	43
4.1.4. Argument Statistic .....	44
4.2. Regional results from indices analysis .....	45
4.2.1. PCA Analysis (8/24/2020 and 9/06/2020 Images) .....	46
4.2.2. NMDI and NDWI Results .....	49
4.3. Susceptibility Scenario .....	51
4.3.1. DEM Results .....	51
4.3.2. Distance Accumulation (DA) Results .....	52

4.3.3. NDVI Results .....	53
4.3.4. Rescale by Function .....	54
4.3.5. Weighted Susceptibility Results (Soft Classification) .....	54
4.3.6. Manual -Hard Classification Susceptibility Results .....	57
4.3.7. Electric Lines .....	59
4.4. Synthesizing and Comparing Different Extents and Resolutions .....	60
4.4.1. Overlaying Susceptibility and Electric Lines Maps .....	60
4.4.2. Comparing Two Scenarios-MODIS Resolution .....	62
4.4.3. MODIS and DEM-PlanetScope Comparison .....	63
Chapter 5 Discussion .....	64
5.1. Discussion .....	64
5.2. Limitations .....	65
5.2.1. NMDI and NDWI .....	65
5.2.2. Multidimensional Analysis .....	66
5.2.3. Susceptibility Analysis and Ground Truthing .....	66
5.3. Future Research .....	67
5.3.1. Model-builder vs. Notebook Environment .....	67
5.3.2. Adding VIIRS product .....	68
5.4. Conclusion .....	68
References .....	70
Appendix: NMDI and NDWI Results .....	75

## List of Tables

Table 1. Data Sources .....	19
Table 2. Spatial References.....	20
Table 3. MODIS Naming Conventions .....	24
Table 4. DEM Data Description .....	31
Table 5. Output from PCA Analysis Bands.....	46
Table 5. Output from PCA Analysis Bands.....	47
Table 6 . Model-builder versus Notebook .....	68

## List of Figures

Figure 1. Carbon Emission from Fires in California .....	2
Figure 2. Atmospheric cross-section acquired by Calipso fly-over on September 7, 2020.....	5
Figure 3. The Map of study area, ArcGIS PRO, Basemap Imagery Layer, LANDSAT.....	7
Figure 4. Workflow Diagram .....	18
Figure 5. Map for Surface Reflectance Bands 2,6, and 7 .....	25
Figure 6. 3D (left) and 2D (right) models for Eikon equation.....	28
Figure 7. Model-builder schema for DEM processing. ....	32
Figure 8. Soft classification and hard classification models.....	34
Figure 9. MODIS Multidimensional Workflow .....	35
Figure 10. Temporal Profile for Bands 2, 6, and 7 Line Boxed Extent .....	36
Figure 10. Temporal Profile for Bands 2, 6, and 7 Line Boxed Extent .....	37
Figure 11. Temporal Profile for Bands 2,6 and 5 Three Sampling Boxes.....	38
Figure 11. Temporal Profile for Bands 2,6 and 5 Three Sampling Boxes.....	39
Figure 12. Trend Analysis Bands 2,6 and 7 .....	41
Figure 12. Trend Analysis Bands 2,6 and 7 .....	42
Figure 13. Predict Raster layers. Channels 2,6, and 7 .....	43
Figure 14. Argument Statistic map for Band 2, Maximum values .....	44
Figure 15. Argument Statistic map for Band 6, Maximum values .....	44
Figure 16. Argument Statistic map for Band 7, Maximum values .....	45
Figure 17. PCA Components 1,2,3, and 4. ....	49
Figure 18. NMDI and NDWI Spatial-Temporal Results.....	50
Figure 19. Distance accumulation maps (ArcView 3D, left, and 2D layout, right) .....	52
Figure 20. NDVI maps for 09/06/2020 (left) and 08/24/2020 (right), PlanetScope Scenes.....	53
Figure 21. Susceptibility maps.....	55

Figure 22. Reclassed Susceptibility maps.....	56
Figure 23. Manually Reclassed Susceptibility maps .....	58
Figure 24. Electric lines .....	59
Figure 25. Synthesized susceptibility maps .....	61
Figure 26. Spatial distribution of NMDI over Southern California and Los Angeles County .....	62

## List of Abbreviations

ANF	Angeles National Forest
AOI	Area of Interest
CRF	Cloud Raster Format
DA	Distance Accumulation
DEM	Digital Elevation Model
GIS	Geographic information system
HDF	Hierarchical Data Format
MODIS	Moderate Resolution Imaging Spectroradiometer
NDVI	Normalized Difference Vegetation Index
NDWI	Normalized Difference Water Index
NMDI	Normalized Multi-Band Drought Index
NIR	Near-Infrared
PCA	Principal Component Analysis
SWIR	Short-Wave Infrared

## **Abstract**

The fire season has lengthened as heat waves induced by global warming have created life threatening conditions around the globe. One of the most affected regions is the West coast of the United States where, in particular, California experiences record breaking fires year after year. This trend is most likely to worsen in the following decades. In order to improve pre-fire detection, the remote sensing platforms use a combination of the integrated small satellites constellation and regular satellite platforms to provide an early warning system. The combined satellite early warning system relies on multispectral and multiresolution satellite networks. This statement of research proposes a fire susceptibility scenario that will attempt to delineate fire susceptible areas from (1) drought indices, (2) prediction, and (3) weighted overlay analysis. In order to avoid reliance 5+ hours latency between data transfer and data processing for state-of-the-art satellites. The proposed methodology of this study is to assess data pipeline from acquisition with a focus on short-interval pre-fire assessment that will delineate potential high-risk areas hence allowing officials to focus preventive measures accordingly. The research aims to improve the short-interval pre-fire data analysis by assessing the Bobcat fire outbreaks and taking a closer look at pre-fire detection methodology. Results from weighted overlay analysis scenarios delineate areas that are classified as susceptible. On the other hand, prediction and drought indices scenarios do not yield expected results.

## Chapter 1 Introduction

The fire season was already putting strain on the Southern California Fire department before the Bobcat fire was initiated. Between August 16-17, 2020 a series of fires were triggered by thunderstorms. Shortly after the extreme episode of Santa Ana dry winds created a record-breaking heat wave that created a mega-complex where multiple fires merged together. With fire departments on strain a possible aid to fire prevention could come from GIS observation and assessment of ground conditions.

Climate and fire experts have predicted that wildfires will grow. Yet, many fire and climate scientists were surprised by the atmospheric environment that caused many of the fires in 2020 (Voiland 2020).

Satellite instruments were helping climate scientists to understand the extent and strength of the wildfires in September 2020. Each weather disaster analysis requires specific computational needs. Monitoring pre-fire conditions on the ground requires data streams from satellite constellations and weather stations. In addition, processing large datasets was time consuming hence scaling down data size without losing crucial information was one of the goals of this study.

Are fire regimes changing due to global warming? There was an apparent upward trend in extreme wildfire events, as shown in Figure 1. In figure 1 on horizontal axis time frame was inserted and on the vertical axis carbon emission units in Tg. Tg stand for tera-gram (1Tg =  $10^{12}$  grams). The fire season has lengthened along with fire intensity and frequency.

In 2020 Bobcat fire burned approximately 115,800 acres while causing unhealthy air quality, property destruction, and multiple freeways closures.

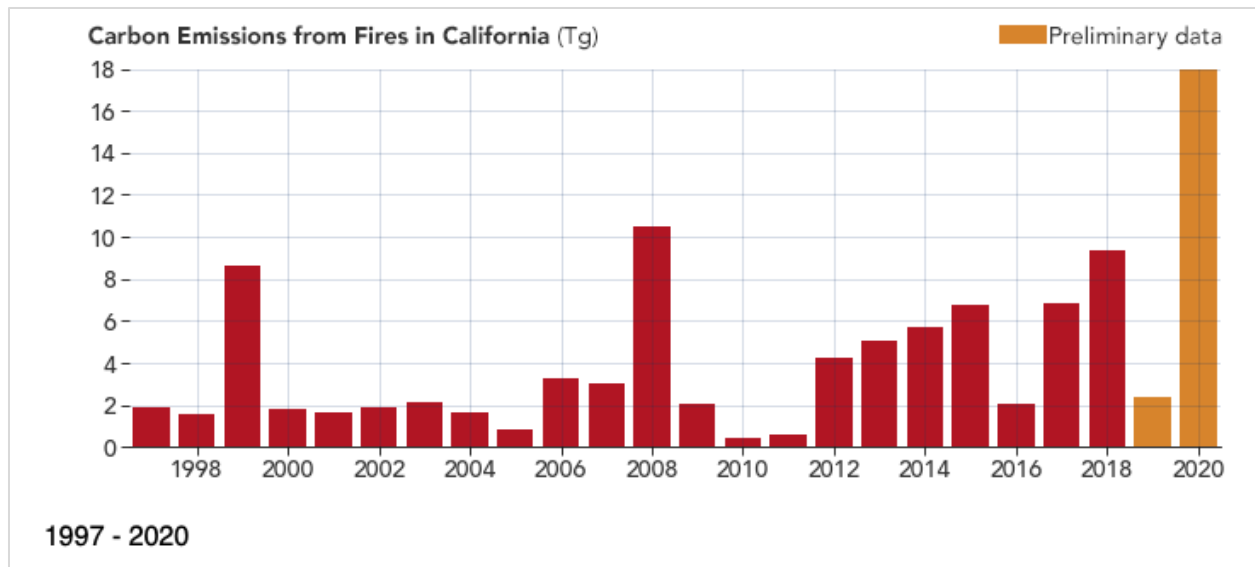


Figure 1. Carbon Emission from Fires in California.

## 1.1. Study Objective

The research motivation was to assess GIS fire detection capabilities of different resolutions and provide a more targeted response by first responders before the fire outbreaks. Pre-fire assessment could delineate locations where the moisture content and proximity to electric cables and road network were classified as more than average hence labeling the regions as more hazardous. In addition, processing large datasets was time consuming hence scaling down data size without losing crucial information was one of the goals of this study.

A hope was that this research will have two potential users: land management agencies and first responders. Land management agencies can adjust development plans for potential fire prone areas while the first responders could delineate fire prone areas and deploy preventive measures.

One key ingredient in minimizing the damage caused by fire was the reaction time. From the moment when satellites acquire images that were classified as fire, then the ground station processing and distributing took 4 to 5 hours (Marder 2019). During the 4 to 5 hours' time frame the fast-moving fire could burn as much as one acre per second of farm, residential, and developing land. The first responders could be more efficient in containing fire if they can obtain pre-fire warnings from a GIS analysis.

## **1.2. Motivation**

The research aimed to simulate the short-term pre-fire data analysis by assessing Bobcat fire outbreaks and taking a closer look at pre-fire detection methodology. Therefore, looking for a potential modification in raster analysis that could delineate risk areas more precisely.

The fire outbreak had happened during the extreme episode of Santa Ana winds. These meteorological conditions were responsible for many fire outbreaks in Southern California. In addition, the weather pattern was related to deteriorating air quality and increased the probability of a quick-fire spreading (Voiland 2020). After burning more than 460 square kilometers of the San Gabriel Mountains in September 2020, the Bobcat fire now ranks among the largest fires on record for Los Angeles County, California. The wildfire initiated on Sunday, September 6 near Cogswell Dam. Supported by shifting wind direction, the fire grew with steady pace over the next twenty days during unusually warm, dry conditions.

### *1.2.1. Fire health Hazard*

A smoke from fire penetrates deep into lungs producing a wide span of health problems. Smoke plums from wildfire carried ozone, carbon monoxide, nitrogen dioxide, polycyclic aromatic hydrocarbons, aldehydes, and particulate matter (PM) less than 2.5 mm in diameter (PM<sub>2.5</sub>) (Naeher et al. 2007). In the paper by Jia (Jia et al. 2014) the authors synthesized over 60

health studies where the connection between health hazard and wildfire was established.

Majority of studies analyzed data from remote sensing platforms by tracking pollutants level (PM<sub>10</sub>). The aforementioned paper explores how climate change amplifies the link between fire occurrences and public health. Another study by Hauptman expanded and suggested that climate effects not only will exacerbate wildfire patterns but they will add the long-term chronic effects that are less studied. In addition, Hauptman pointed out that children's developing lungs are more susceptible to lung damages (Hauptman, Balmes, and Miller 2020).

Health studies required a longitudinal approach; thus, this study drew similarities with previous fire episodes. One of these fire episodes happened in Northern California in 2008. The Northern California 2008 fire complex was composed of many fire patches burning at the same time and lasted for 42 days. The study region (Reid et al. 2016) included the San Francisco Bay Area, the Sacramento Valley, Lake County, the Mountain Counties, the North Central Coast, and the northern part of the San Joaquin Valley. Due to its widespread spatiotemporal extent this fire complex, according to Reid, represented a relatively solid case to study hospitalizations and asthma triggered by wildfire exposures. In this study as in previous studies (Delfino et al. 2009; Henderson et al. 2011) a model found substantial increase in asthma and hospitalization that was caused by PM<sub>2.5</sub>.

Additionally, to long and intermediate health effects studies that often require years to complete, the immediate health hazard was obvious from the smoke plume that was recorded by NASA's Calipso instrument on September 7, 2020, in Figure 2. On the upper right corner of the atmospheric cross section we can see the satellite orbital path. The path passed over the Bobcat wildfire outbreak.

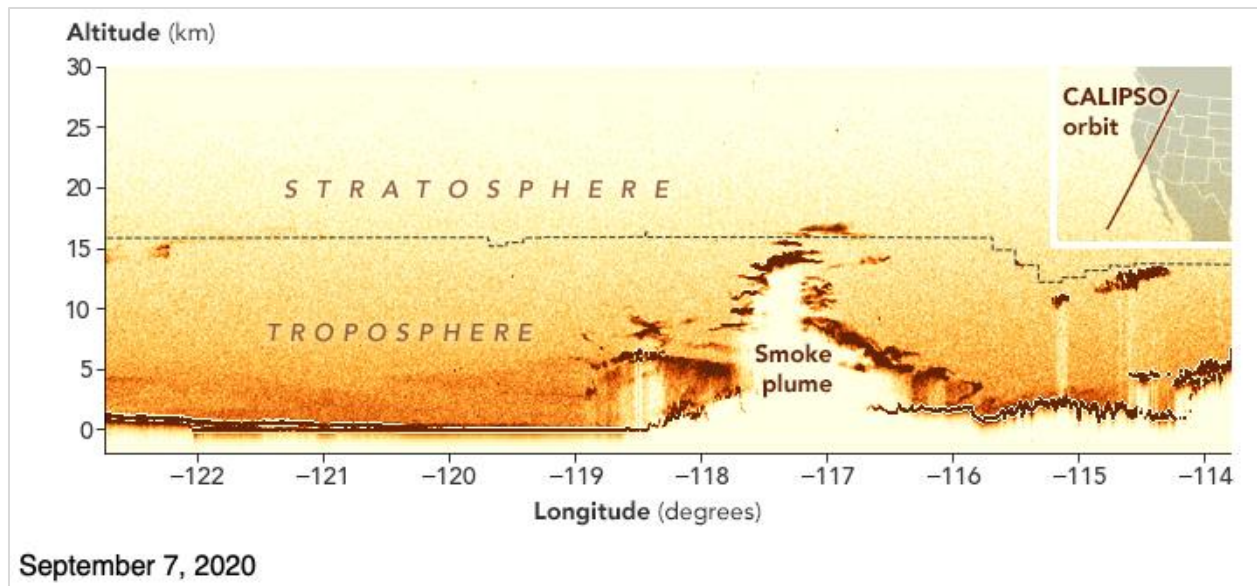


Figure 2. Atmospheric cross-section acquired by Calipso fly-over on September 7, 2020.

### 1.2.2. Fire Advisory

Delivering near-real time fire data is provided by NASA's Fire Information for Resources Management System (FIRMS). The system issues Near-Real Time (NRT) fire data at an approximately 3 hours' time window. MODIS and VIIRS platforms are used by NASA FIRMS for fire detection. While both platforms complement each other, Krishna Vadrevu and Kristofer Lasko's comparison between two platforms pointed that VIIRS fire detection was between 4.8 and 6.5 times higher than MODIS platform (Vadrevu and Lasko 2018). However, this project was focused on pre-fire assessment, and MODIS platform datasets were used to observe the region on the coarser scale. MODIS product will be discussed in more depth in Chapters 2 and 3. In addition, the study introduced the viability of high-resolution data from Planet small satellite constellation.

### 1.3. Study Area

Bobcat Fire most likely happened when tree branches touched the electric lines. A more in-detail analysis could map areas where electric lines proximity to vegetation could be classified as hazardous. Hence, local authorities could have intervened and perhaps prevented the event.

Bobcat fire outbreak occurred North of Downtown Los Angeles at West Fork of San Gabriel Canyon at Cogswell Dam which is part of Azusa, CA (Figure 3). The most likely culprit was tree branches touching an electric transmission line that is operated by Edison Power Company. In addition to the spatial randomness of this event, it was important to describe the highly extreme weather conditions that made the whole environment highly prone to the wildfire outbreaks. Climate was controlled by Pacific air masses where the summers are dry and sunny and winter months received all the rainfall, according to Cities of the United States (Los Angeles: Geography and Climate). During the fall and winter months the prevailing high-pressure system in the Great Basin created Santa Ana winds. The winds started to blow from the cold dry air mass in the desert areas towards the Pacific. These meteorological phenomena affected a couple of major metropolises such as Los Angeles, San Diego, and Mexicali (Alvarez and Carbajal 2019). Just before the fire outbreak, there was a disaster waiting to happen. Prolonged drying and heating of both local vegetation and air triggered multiple fires that have surpassed the previous California record for the number of square kilometers burned in one year. Bobcat's exact coordinates were pinpointed to 34.241 latitude, -117.868 longitude according to Cal Fire Department.

Los Angeles County was home to around 10 million people in 2020. Together with southern Orange County and Riverside the population number jumps to 13.8 million which makes one of densest urban sprawls in the United States. Despite the high population density of

Los Angeles County, the fire, in general, stayed away from urban areas. In addition to meteorological conditions local topography played a role in fire susceptibility. Slope terrain tends to accelerate fire spreading due convective heating. Los Angeles topography was shaped by various tectonic processes. L.A. County is situated in the basin that is created through tectonic subsidence during a three-stage evolution process (Ingersoll and Rumelhart 1999) and as such its topography exhibits high variability in elevation distribution.

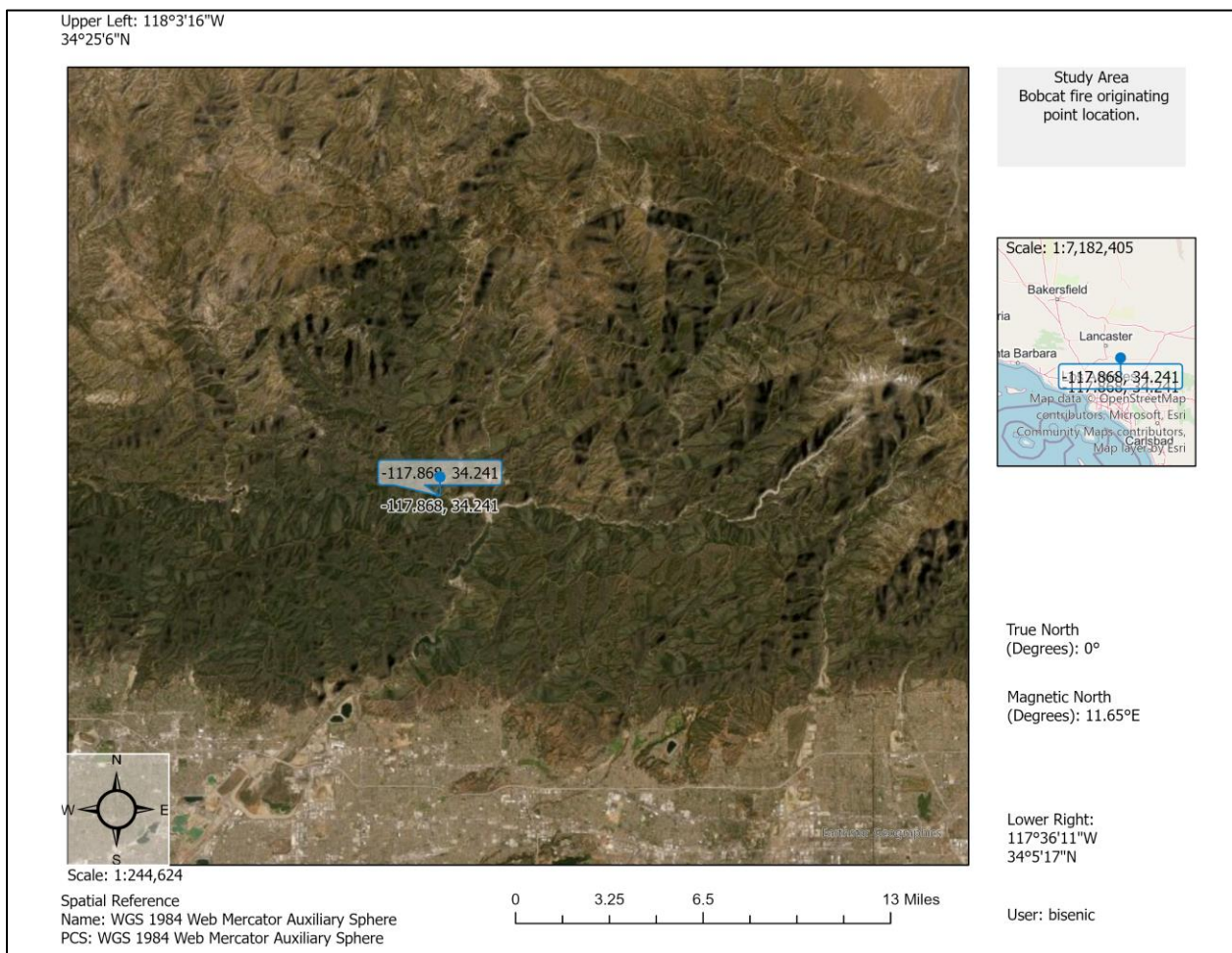


Figure 3. The Map of study area, ArcGIS PRO, Basemap Imagery Layer, LANDSAT.

## **Chapter 2 Literature Review**

Substantial reporting on the Bobcat Fire outbreak has been produced since the event took place on September 6, 2020. Chapter 1 introduced specific reports produced by NASA that showed the magnitude of damage caused by Bobcat fire. The following chapter is divided into regional context, relevant studies for weighted pre-fire susceptibility assessment, and resolution problems. This report explores ancillary research that subdivides each of the previously mentioned divisions into subcategories.

### **2.1. Regional Context**

When drying happens, both dead and living green cover dries out and become more combustible. Thus, the likelihood of ignition increases together with the fire spread. As drought continues then the number of days with higher vegetation flammability and fire spreading rises. There is a growing consensus among policymakers and land management agencies that developing new wildfire mitigation strategies is necessary to mitigate the growing cost of fire suppression. The U.S. Department of Agriculture and Forest Service projected that the cost for fire suppression will reach USD 1.8 billion per year. This estimate was done in 2015 (U.S.D.A. Department of Forest 2015).

In the study by Salguero et al. 2020 the authors pointed out that interconnectivity between manmade and natural factors have increased wildfire occurrences. The study concluded that the wildfire occurrences have been increasing over the contiguous United States (CONUS). The California region is not an exception to the trend, moreover figure 1 suggests that California wildfire regimes are accelerating. However, due to a wide spatial extent demarking area with high fire occurrence require creating Fuel Management Zones (FMZ). This approach is described in detail in the study by Afonso and colleagues in 2020 (Afonso et al. 2020). Their work used a

machine learning approach where the variable size buffers are created around manmade infrastructure. The study is located in central Portugal.

FMZ method created an interconnected web of fire prone areas. Due to coarse spatial resolution of the MODIS platform this project observed the fire fuel accumulation in a regional context. A similar approach was done in paper by Littell and colleagues in 2016 where authors evaluated fire changes of different parts of North America. They concluded that there is a complex interplay between drought and fire. While drought (Littell et al. 2016) is a main contributor for fire events the local factors such as type of tree and tree morphology accelerate or buffer fires regimes.

This study observed fuel accumulation while using MODIS satellite 500-meter pixel resolution. At this pixel resolution creating FMZ did not seem as a viable strategy due to a coarser spatial resolution when compared to Sentinel 10-meter pixel resolution. However, the scenario-based approach did observe Southern California region fuel accumulation and surface reflectance fluctuations by creating multiple indices and raster predictive models that will be discussed in next sections.

### *2.1.1. Multidimensional Data*

The concept of Big Geospatial data with near-real time image streaming capabilities provides an early warning system for disasters such as wildfire outbreaks (Goodchild 2018). According to Goodchild, patterns derived from big data are replacing traditional empirical approaches with simulations powered by algorithms. This project used big data and pattern detection algorithms in order to extract information that would otherwise be time consuming for one person.

Large amount of climatological and meteorological data was collected and stored in space-time cubes. Retrieving useful information that could signal a potential fire hazard from space-time cubes is best achieved by packing data in gridded multidimensional data format. The space-time cubes are gridded multidimensional datasets packed in GRIB, NetCDF, and HDF file formats. This thesis used HDF data formats. Also, this packaging allows for a large volume of data to be retrievable and displayable in GIS software such as ArcGIS or IDRISI TerrSet (Xu et al. 2016). Xu and colleagues also pointed out that NOAA and NASA HDF datasets have shown great utility when visualized and analyzed with GIS platforms such as ArcGIS. Daily temporal coverage and wide spatial extent of NASA's data from MODIS provided an excellent testing ground for utilizing these instruments on the Los Angeles County scale.

### *2.1.2. Pre-Fire Indices*

Multiple studies focus on detecting signals in the physical environment so the damage from the fire outbreak could be minimized or even prevented. Possible pathway to early warning was to create map products that utilize indices derived from RS platforms. In the literature review paper Barmpoutis and colleagues (Barmpoutis et al. 2020) point out that as of 2020 the current state-of-the-art fire detection technology uses Sun-synchronous satellites MODIS and VIIRS for fire prediction. The fire prediction is relying mostly on normalized difference vegetation index (NDVI), land surface temperature (LST), and temperature extremes. The aforementioned paper also assessed the efficiency of small satellites with respect to fire and smoke detection. The Bobcat wildfire project assessment used a similar approach. This project used selected satellite-derived indices the normalized multi-band drought index (NMDI) and normalized difference water index (NDWI).

NMDI index fitness for use is discussed by Lingli Wang and John J. Qu (2007) where the findings suggest that fitness for use is highly dependent on vegetation density and soil type (Gu et al. 2008). NMDI is proposed in 2007 by Wang and Qu (2007) for remote sensing of water content from satellites. The aforementioned index returns a more precise pixel value for drought severity. A drought severity index is successfully used by many researchers and responsible agencies to forecast fire hazard. This study used a top down view from MODIS satellite using NMDI and NDWI indices. Forecast, in this form of pre-fire warnings, are often used by FIRMS (Fire Information Management System) where the MODIS and VIIRS satellites are tracking thermal anomalies across the globe. Similarly, to this approach, this project used NMDI and NDWI indices to track water content anomalies across the Southern California region.

The previously mentioned authors point out that NMDI and NDWI have been used to track soil moisture deficit which is directly related to plants' health, when studying fire outbreaks in Georgia, USA, and southern Greece in 2007. Wang and his colleagues focused their study on NMDI, NDWI, and Normalized Burn Ratio (NBR) (Wang and Qu 2008). A study by Xu and colleagues (2008) that is not directly involved in pre-fire assessment complimented Wang's study by testing how the aforementioned indices respond to site measured water content fluctuations. Xu and colleagues concluded that indices accuracy is highly dependent on soil type and soil's diversity.

Wang and Qu (2007) used MODIS satellites to compare the efficiency between NMDI, NDWI, and NBR. NMDI has a higher detection rate and it is able to delineate fire spots more accurately using NIR and SWIR bands. Even though this study was focused on detecting pre-fire conditions, this approach appears applicable for observing ground drought conditions prior to

fire outbreak. Multiple studies have identified the drought, water soil content and humidity, as governing variables in wildfire occurrences (Farahmand et al. 2020; Litell et al. 2016).

### *2.1.3. Data Transformation*

This thesis worked with a large volume of data. Therefore, computational requirements pose a challenge when it came to time needed to complete analysis and storage needs. In order to reduce computational requirements this project explored previous publications on principal component analysis (PCA). Rokni and colleagues (Rokni et al. 2016) study of surface water changes applies an analytical method using data storage saving methodology. The aforementioned methodology used indices, NDWI, NMDI, Water Ratio Index (WRI), and NDVI. This data saving approach, named principal component analysis (PCA), used LANDSAT ETM + datasets, with three images from August 2000 and three images from July 2010. Images covered the study area of lake Urmia in NW Iran. The surface water change was computed using PCA transformation. PCA analysis was used for dimensionality reduction while at the same time this analysis preserved the variance within the dataspace. This method can be refined and used for lowering datasets size. Rokni's paper pointed out that each image can be processed separately or all images can be merged together creating a multitemporal dataset and then PCA can be applied on a composite image. Both approaches were explored in the study. Further, each image was classified and processed independently and then overlaid and compared on pixel by pixel scale. The methodology and results were discussed in chapter 3 and 4.

## **2.2. Relevant Studies for Weighted Pre-Fire Susceptibility Scenario**

On the parallel track the thesis performed the pre-fire susceptibility assessment. Previous research has found a strong correlation between topographic features and fire susceptibility. In addition, when topo features were combined with atmospheric and land cover data then fire

prone areas can be delineated with a higher confidence level. In the paper by Salis (Salis et al. 2014) the authors synthesize atmospheric, topographic, Digital Elevation Model (DEM) layer and its derivatives; Slope, Aspect, and Hillshade, and land cover type with a goal of creating a fire prediction model in Sardinia. The island that is located in Mediterranean basin, Italy.

Similarly, this research integrated the aforementioned variables and it attempted to produce a wildfire suitability model. Contrary to Salis's approach where they observed a wider spatial-temporal range a wildfire suitability model focused on a narrower spatial-temporal extent. Therefore, the study planned to modify methodology adopted by Salis et al. (2014) and used a two-week period right before the fire outbreak. The fire prediction model developed for Sardinia did not utilize satellite imagery but this project's goal was to run a weighted susceptibility scenario with Planet 3 m resolution imagery with DEM 30 m resolution.

Even though higher resolution was computationally taxing, a higher resolution or the pixel size influenced the detection accuracy of the fire prone areas. As suggested by Salajanu (Salajanu and Olsen 2001) smaller pixels increased overall accuracy. Salajanu and Olsen assessed pixel size in respect to land cover classification when LANDSAT imagery was integrated with the SPOT-XS (1.5 m and 6m resolution) platform.

### *2.2.1. Angeles National Forest Site Selection for Fire Susceptibility Scenario Using Planet and DEM Data*

The Bobcat Fire initiated in Angeles National Forest covering an area of approximately 470 square kilometers. The immediate surroundings of the fire outbreak location had a couple of roads and electric lines passing through. Road and electric networks intersected the vegetation and high slopes at numerous locations. Delineating these touching points was doable with finer pixel resolution. Finer scale allowed more accurate classification in transitional zones between vegetation and non-vegetation covered areas. Delineating transition from vegetation covered to

non-vegetation covered patches was done by using NDVI index. This project used PlanetScope data small satellites cubes that provide 3-meter pixel resolution at the footprint size. This RS platform performance was tested against LANDSAT 8 and Sentinel products where all three products are compared to LIDAR extracted tree canopy heights in temperate climate (Shimizu et al. 2020). In experiment by Csilik (Csilik, Kumar, and Asner 2020) Planet Scope products were tested again against LIDAR data for canopy height in tropical forest in Peru. Shimizu's paper suggests that Planet data was more suitable for finer spatial resolution and in some cases where the model was compared against Sentinel-2 data, Sentinel-2 achieved better results. On the other hand, Csilik research has shown that Planet's data jointly with DEM datasets can estimate tree canopy with RMSE at 4.6 m for tropical forest using a regression model analysis.

### *2.2.2. Adding DEM Data*

The previous research suggested that slope and aspect play a significant factor in fire spreading. If the terrain was relatively flat then the fire spreading tended to slow down while steeper terrain favors a quicker fire spreading. This was mostly due to pre-heating in an uphill direction (Rothermel 1983; Mermoz et al. 2005; Verde 2008).

Bobcat fire started in Angeles National Forest which is part of the San Gabriel Mountain system. With the region's specific topography, climate, and vegetation that draws similarities with Sardinia's wildfire exposure risk modeling (Salis et al. 2014). This research plans to modify Salis' approach and apply DEM data into fire susceptibility analysis.

In order to add a 3rd dimension to this study, integrating a DEM and using DEM derivatives such as Slope, and Hillshade adds information to the final map products.

DEM is served by USGS with standard file formats; IMG, Grid Float, and ArcGrid (Table 4).

The mapping was originally done with the Space shuttle mission back in 2000. Shuttle Radar

Topographic Mission (SRTM) used two radar antennas and one fly-over to produce a digital elevation model with remote sensing techniques interferometric synthetic aperture radar (InSAR). With spatial resolution at around 30 m, this dataset has been used to derive slope, aspect, and hillshade.

Sardinia's wildfire exposure analysis synthesized Slope, Aspect, and Hillshade with fuel types in the ArcFuel platform. When overlaid with a shapefile that had land usage datasets such as forest type, urban areas, water bodies, and grasslands, then DEM data, according to Salis (Salis et al. 2014), produced a weighted map. A map displayed dead fuel content from low to moderate.

### **2.3. Scale and Resolution Problem**

Observing pre-fire conditions in the Bobcat-fire region included multiscale observations. In the paper by Goodchild (2011), the author evaluated the meaning of scale and how scale dependency transcended geographical features and influenced their representation on the map. As we zoom in, relatively blurred features were becoming more visible and delineation occurred hence individual features were becoming easier to distinguish. The tradeoff between various scales was discussed (Avelino et al. 2016) in previous publications. The governing variables for fire indices operated simultaneously at various scales and the magnitude of influence varied between the scales. Also, previous studies by Avelino suggested that a higher resolution did not necessarily lead to a better analysis. Understanding the appropriate scale of analysis often required testing analysis on multiple scales to check for potential biases.

The attempt to track these processes had to include multi scale analysis while finding the model that had the best fit for the aggregation method. Since there were only two available images from LANDSAT satellite for the studied time period, the project opted out from this

approach. Because, creating a linkage between various scales and lowering the Modifiable Areal Unit Problem (MAUP) this study needed temporal continuity with the LANDSAT 30-meter resolution data sets. MAUP has been a widely discussed problem in the GIS community. MAUP is a data aggregation problem. In general, it has zonal and scale effects. In scale case point data or pixels were aggregated to a specific areal unit or data from one scale was analyzed at another areal scale. Multiscale analysis, as discussed by Jelinski and Wu (2000), explored the relationship between data pattern and scale. This study concluded that the relationship between pattern and scale is evasive. Jelenski and Wu (2000) used two approaches when assessing multiscale analysis of landscape pattern; indirect and direct. Indirect methods use a more general pattern with classified data while direct methods rely on statistical methods.

### *2.3.1. Tradeoff Between Resolutions*

In addition to the MAUP problem there were sensor resolution limitations. In the paper by Boyd and Danson (Boyd and Danson 2005) the authors discussed the challenges when 1 km resolution is used to differentiate between forest and non-forest areas. The authors describe the attempt to find a relationship between forest variables and spectral signature. They point out that while looking for biomass reflectance in near infrared (NIR) research could not find a significant relationship but once they utilize middle infra (SWIR) they did find a strong relationship between reflectance and the forest's biomass.

Since the resolution was around one square kilometer then from the information stored in the pixel it was not easy to extract and pin point where the forest was dissipating and transforming into a meadow, for example. Similarly, to 1 km, 500 m resolution cannot precisely delineate transition zones between forest and non-forest covered features. The coarse resolution for the global observation made this delineation tricky in transition zones. This issue

was evident in Bobcat's area topographic layout. The layout composition contained many green forestry patches that frequently were interrupted with bare soil features. Therefore, the surface reflectance signal at 500 m resolution contained a mixture of reflectance from bare soil, roads, and vegetation covered areas. Even though high-resolution data can aid this problem, processing and storing was computationally too intense.

In general, the tradeoff between resolutions created dynamical interplay between variables where an increased spectral resolution allowed sensors to receive shorter wavelengths. Hence radio waves detection dropped and even became invisible after a certain threshold, while the problem with brightness detection arose. In the case of spatial resolution, the focus is on the minimum distance between two objects that can be separated and identified, a forested and deforested area (Boyd and Danson 2005). If the study needs an improved level of detail then satellite derived data needs to have a lower altitude flight path or study needs access to high resolution sensors from satellite or drone, or both. In both cases, the cost jumps substantially (Hendel and Ross 2020).

In addition, there was a physical limitation of sensor's size because the sensor optical receivers were calibrated for certain wavelengths and if optical receivers were designed for longer wavelengths, then shorter wavelengths were not captured by the sensor. As discussed by Cambell and Wynne in their book (Campbell and Wynne 2011), the surface of a digital camera is an array of photosensitive cells and each cell captures the energy from arriving photons. Also, the size of array and the size of each cell, within the array, controls the resolution of the sensor. Consequently, the larger cell can capture more photons and produce more electrons. This feature allows imaging in low energy environments while at the same time compromises spatial resolution because the image surface is occupied with fewer cells (Campbell and Wynne 2011).

## Chapter 3 – A Scenario Based Evaluation Framework for Fire Hazard Assessment

This chapter presents data sources and methodology used in this study (Figure 4). The first part introduced data sources. In the second part the study laid out the workflow for regional indices analysis with IDRISI software and multidimensional raster prediction analysis with ArcGIS Pro. The third section of this chapter focused on local extent where data processing techniques were discussed in the context of producing Distance Accumulation, Electric Lines, DEM derivatives, and NDVI layers. Further all aforementioned layers from local extent were synthesized. Therefore, three parallel analyses, data transformation, raster prediction and fire-susceptibility analysis, were performed side by side.

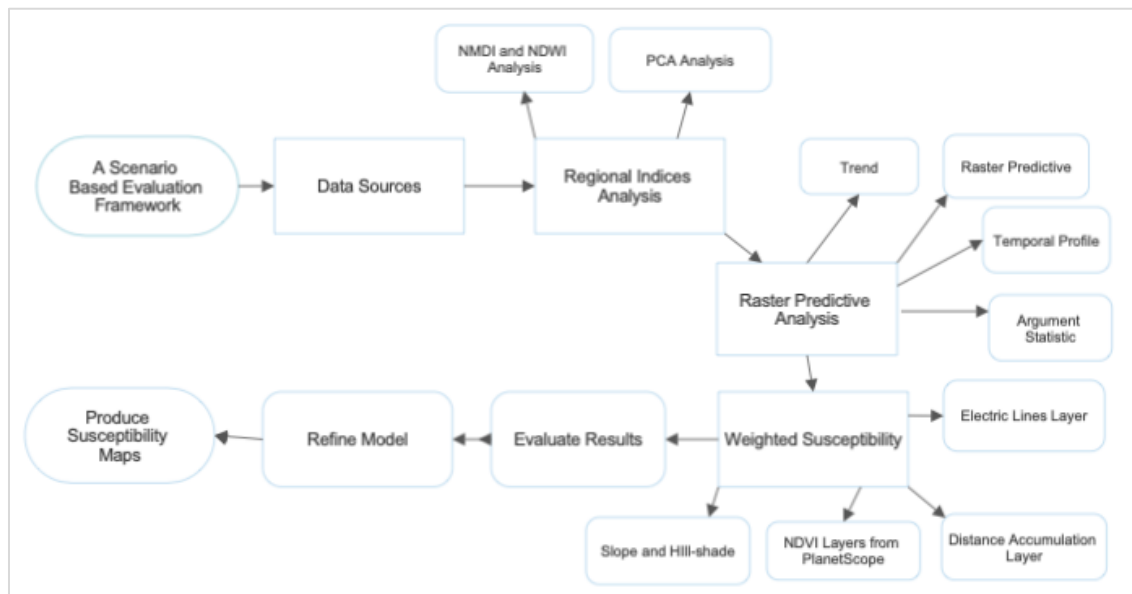


Figure 4. Workflow Diagram.

### 3.1. Data Sources

Planet data was downloaded from the planet.com explorer was used for imagery analysis. The images were corrected for surface reflectance. The time scale was set from 08/24/2020-09/07/2020. From the two weeks' time range there were 7 dates for which satellites captured the

full extent. During the flyovers on other dates the images covered between 22%-84% of targeted area. Insofar Planet’s 3 m resolution data was not used for fire susceptibility analysis. This study expected that when high resolution data was overlaid with electric lines, road network, and slopes then a weighted map would delineate more precise fire susceptible areas.

Datasets	Spatial (Resolution)	Temporal Resolution (2020)	Description	Data Type	Bands	Precision	Accuracy	Source
Planet	3.7 m	1 day		Geo-TIFF Raster File	Band1(455-515nm) Band2(500-590nm) Band3(590-670nm) NIR (780-860nm)	Dictated by Ground Sampling Points and Radiometric Correction Scale (20x8) km	Cloud cover or smoke can affect accuracy thus the captured image can have ex. 25% cloud cover. Datum	<a href="https://www.planet.com/explorer/">https://www.planet.com/explorer/</a>
MODIS	500 m	1 day		HDF Multidimensional Dataset	Band 7(2105 – 2155 nm) Band 6 (1628 – 1652 nm) Band 2 (841 – 876 nm)	Dictated by Ground Sampling Points and Radiometric Correction	Cloud cover or smoke can affect accuracy thus the captured image can have ex. 25% cloud cover. Datum	<a href="https://search.earthdata.nasa.gov/search">https://search.earthdata.nasa.gov/search</a>
Road Network	N/A	N/A	Tiger Shapefile TIGER Shapefile 2019 Primary and Secondary Roads State-Based Shapefile	Shapefile, geometry polyline	N/A	Dictated by ground sampling points	Dictated by datum	<a href="https://catalog.data.gov/dataset/tiger-line-shapefile-2019-state-california-primary-and-secondary-roads-state-based-shapefile">https://catalog.data.gov/dataset/tiger-line-shapefile-2019-state-california-primary-and-secondary-roads-state-based-shapefile</a>
Electric Gridlines (Edison Power Company)	N/A	N/A		Shapefile, geometry polyline	N/A	Dictated by ground sampling points	Dictated by datum	<a href="https://www.arcgis.com/apps/webappviewer/index.html?id=05a84ec9d19f43ac93b451939c330888">https://www.arcgis.com/apps/webappviewer/index.html?id=05a84ec9d19f43ac93b451939c330888</a>
DEM	30 m	N/A		Geo-TIFF Raster data	SAR	Dictated by topographic features	Dictated by datum	<a href="https://apps.nationalmap.gov/downloader/#/">https://apps.nationalmap.gov/downloader/#/</a>

Table 1. Data Sources.

Electric lines datasets was in shape file format and it is served by California Energy Department webpage and Edison company. Coordinate system is WGS 84 and the last data

update occurred on February 24, 2021 (Table 1). Also, TIGER shapefile was downloaded from data.gov web page and spatial reference was set to CA State Plane NAD 83 coordinate system (Table 2). Both layers were used for susceptibility analysis. As previously discussed, most wildfires were triggered by human error or manmade infrastructure. On a few occasions extreme weather events such as lightning strikes were responsible for a fire outbreak, as happened with the North Complex fire in 2020. However, the majority of the wildfire can be directly or indirectly tracked down to human error (Verde and Zezere 2010; Beighley 2009).

Dataset	Geographic Coordinate System	Projected Coordinate System
Planet	WGS84	WGS84 UTM Zone 11N
MODIS	WGS84	Sinusoidal Projection
Transmission Lines	NAD 1983	NAD 1983 UTM Zone 11N
TIGER/Roads	NAD 1983	WGS UTM Zone 11N
DEM	NAD 83	NAD 1983 UTM Zone 11N

Table 2. Spatial references.

### 3.2. Regional Analysis with IDRISI Terr-Set

The study site for the Bobcat fire outbreak stretched from the West Fork of San Gabriel Canyon at Cogswell Dam in the Angeles National Forest. Due to its relatively small extent, around 118,000 acres, Terra Satellite needed only one overpass in order to capture the full extent (Giglio et al. 2018; Oguro et al. 2011). The Terra satellite has 2330km cross track by 10 km along track at nadir (Csiszar et al. 2014; Shoreder et al. 2014).

Also, due to its high temporal resolution (Adab et al. 2016) MODIS instrument was widely used to estimate vegetation content over a chosen time scale. The study chose a two-week period prior to the fire outbreak and data was downloaded from NASA's Earthdata portal as HDF file format. The Government Data Provider Formats import option was used where the MODISCONV tool worked to import HDF files for a 14 days period. Since, HDF was a

multidimensional raster each day produces seven reflectance bands. MODISCONV tool generated 210 files that included IDRISI. rst raster file formats and supporting RDC files. Out of 105 raster files, the study needed NIR and SWIR images which included surface reflectance bands 2,6, and 7.

Downloaded MOD09GA products were corrected for atmospheric conditions such as Rayleigh scattering, water vapor, gasses, and aerosols, and the product was ready to use.

### 3.2.1. NMDI and NDWI Analysis

Having three bands per day on the 14 days' time span this task had to create a NMDI raster expression which contrary to NDWI indices (Gao 1996) was less centered around single liquid water absorption wavelength. This comparison and equation were derived by Wang et al. 2008, in equations 1 and 2.

$$(1) \quad NDWI = \frac{NIR - SWIR}{NIR + SWIR} = \frac{B2 - B6}{B2 + B6}$$

$$(2) \quad NMDI = \frac{B_2 - (B_6 - B_7)}{B_2 + (B_6 - B_7)} = \frac{0.86\mu m - (1.64\mu m - 2.13\mu m)}{0.86\mu m + (1.64\mu m - 2.13\mu m)}$$

The Raster Calculator created NMDI images for each day by using the difference between two water absorption bands, B6 and B7 (1.64nm and 2.13nm). This index offered an estimation for both soil and plant water content hence this index provided a more detailed estimation of drought condition and fire susceptibility. The normalized multiband index, proposed by Wang and Qu (2007), used bands focused around 0.86nm or Band 2 which were tuned for leaf water detection changes.

Since there was no batch processing option in IDRISI each NMDI image had to be processed individually with IDRISI GIS Analyst tab and Image Calculator option. Interestingly, the IDRISI image calculator does not read files that are displayed on the TerrSet Explore file menu. Thus, this task used the browsing tab to reconnect to the file folder where HDF files were

extracted. Then, by re-connecting to the originally extracted HDF files the Image Calculator was capable of inserting images and calculating NMDI. At the same time, the initiated re-connection displayed the files in the TerrSet Explorer file menu along with already displayed files. Actually, these were the same images just coded differently. It was not clear why IDRISI software had this unnecessary extra step. With 51 images to process this work took approximately 2 hours to complete.

Additionally, this project created NDWI indices. NDWI has shown its utility for drought observation and in early warning for wildfires in various studies (Gu et al. 2007; Ceccato, Flasse, and Gregoire 2002). This satellite derived index combined NIR and SWIR. NIR has shown sensitivity to leaf internal structure and leaf dry matter content but not by liquid water presence. On the other hand, SWIR has been able to detect fluctuations in both vegetation water presence and the spongy mesophyll structure in vegetation canopies (Gao 1996).

### *3.2.2. Principal Component Analysis -PCA*

The PCA technique in its essence was used for dimensionality reduction. Since an average image carries so much data every processing requires a substantial amount of time. Therefore, image analysts wanted to reduce volume of data while preserving fitness for use. By looking for an optimized linear combination between bands PCA process looked for variations between bands that can be related to pixel values within an image.

From the equation (3), below, it was clear that this procedure was dependent on the coefficient's value.

$$(3) \quad A = C1X1 + C2X2 + C3X3 + C4X4$$

X1, X2, X3, and X4 were pixel values for four spectral channels and C's are coefficients related to each channel (Campbell and Wynne 2011). Once PCA was performed then

reconstructing the bands with inverse T-Mode where the goal was to exclude components that represent the noise

### **3.3. Raster Predictive Scenario**

The goal of this approach was to step back two weeks prior to fire outbreak and observe fineness in pre-fire assessment with a goal to detect a signal from the satellite imagery that could indicate a potential high fire hazard.

The key for developing a solid raster predictive model was having data continuity on the time scale and surface reflectance products that covered the NIR and SWIR part of the spectrum.

The MOD09GA product delivered an estimate of the surface reflectance of Terra Moderate Resolution Imaging Spectroradiometer (MODIS) Bands 1 through 7. Images were corrected for atmospheric conditions such as Rayleigh scattering, water vapor, gasses, and aerosols. Observations were provided along with the 500-meter (m) surface reflectance. The reflectance data from the MOD09GA were used as the source data for many of the MODIS land products. Dataset contained 15 granules and the data format was HDF. Images were captured daily and each image contained a date and time stamp. Even though MODIS instrument was designed by NASA to track changes on a large scale there was apparent utility on the smaller, county, scale. Usefulness of MODIS data was apparent when integrated with GIS platforms such as ESRI and IDRISI. This thesis used IDRISI and ESRI platforms to utilize MODIS imagery.

#### *3.3.1. Creating Mosaic Datasets*

MODIS data was stored in an HDF format that was collected over multiple times. The file was downloaded from NASA's Earthdata portal where the time range was set between 8/24/2020 and 9/6/2020.

In order to display multidimensional raster in ArcGIS Pro, first an empty mosaic dataset had to be created. Once the empty bucket was created then adding raster to the mosaic allows specifying the type of dataset that was added. In this case HDF file format was selected from the drop-down menu which automatically allowed parametrization. ArcGIS was now connected with a file and read data from the file hence by choosing one image from the file ArcGIS Pro was capable of displaying all the variables from a multidimensional raster layer. Each one represented a different set of data that can be used for analysis or visualization, and the HDF file for this dataset had 22 variables in total of which 7 were surface reflectance bands. Table 3 showed how naming conventions packed product information.

(MOD09GA.A2020237.h08v05.061.2020343112804.hdf)

MOD09GA	Product Short Name
A2020237	Julian date of Acquisition
h08v05	Tile Identifier (horizontal XX vertical YY)
2020343112804	Julian Date of Production (YYYY DDD HH MM SS)
hdf	Data Format

Table 3. MODIS Naming Conventions.

In addition, creating mosaic datasets from MODIS imagery required more processing time than initially anticipated. MODIS data occupied 1.36GB of storage space hence creating mosaic datasets for each band and rendering images required on average 10-15 minutes for each set. There was apparent time processing growth as more mosaic datasets were added. Band 2 (841-876 nm), Band 6 (1628 - 1652 nm), and Band 7 (2105 - 2155 nm) were displayed in Figure 5. Band 2 was NIR while Bands 6 and 7 were in short infrared SWIR.

Each map used 09/06/2020 as a displayed date. This was a feature of ArcGIS Pro where multidimensional layers can be displayed based on date. Maps were displaying reflectance from bands 2, 6, and 7, where on the central portion of the map right above the fire outbreak point clouds and cloud shadows were visible.

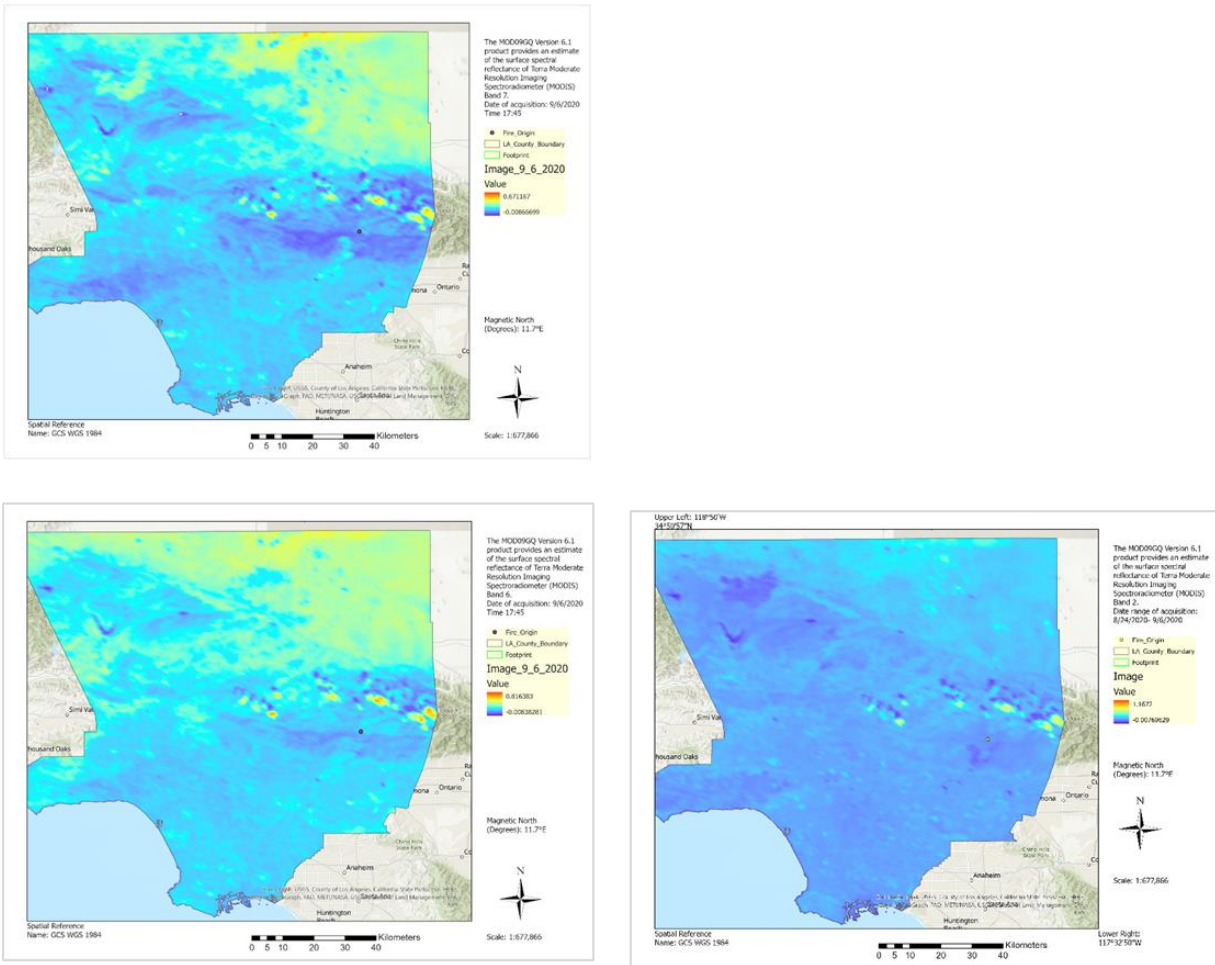


Figure 5. Band 7(2105 – 2155 nm), upper left, Band 6 (1628 – 1652 nm) down left, and Band 2 (841 – 876 nm) down right.

Even though the data cube model, HDF was well-utilized for packing large amounts of data yet data handling was not so straightforward.

During the first attempt, multidimensional had all seven bands integrated into one mosaic dataset. However, displaying and rendering such a big amount of data was time consuming and by breaking it down into seven different mosaiced dataset with one band for each set. The resulting products were capable of rendering images from HDF format. Multidimensional data covered date range from 8/24/2020 - 9/06/2020. Each layer processing extent was set to the LA County boundary extent thus preserving GPU processing requirements. In addition, raster processing was checked to Calculate statistics and build pyramids in the processing template. In total seven mosaic datasets are created, one for each band.

On the side note, multiple attempts to produce NMDI indices did not produce results. Generating index from Multidimensional processing template produced a raster layer that was composed from two bands but the value did not correspond to equation; moreover, the ArcGIS Pro processing template took maximum and minimum reflectance value and displayed them on the value chart. Apparently, this study could not create processing template, in ArcGIS Pro, to calculate NMDI from multidimensional raster.

MODIS's instrument Multidimensional data were processed with workflow that was borrowed from NASA's Earthdata documentation page (Madden 2020). The workflow in the Figure 8 shows the steps this thesis took in order to extract a pattern in data that could lead to an early pre-fire signal. From the spatial extent of Los Angeles county this study wanted to find area coverage that could be further analyzed with a finer spatial resolution.

A model for raster predictive analysis was developed with the Lucidchart app. Figure 9 shows the path for developing Trend, Predict, and Anomaly analysis. As shown in Figure 9, the results for Predict depended on Trend result and Anomaly results depended on Predict results.

On the other hand, Argument Statistic and Temporal Profile results were produced from raw data.

### **3.4. Weighted Fire Susceptibility Scenario with Planet-Scope Imagery, DEM derivatives, Electric Lines, and TIGER/Roads Shapefile**

From Los Angeles County two weeks spatial-temporal extent this thesis zoomed in to approximately 10 km by 10 km extent in Angeles National Forest region, thus narrowing research to a finer resolution while using reverse engineering methods. Since, the fire already happened and by knowing the location, the study looked into surrounding man-made infrastructure, topo-features, and fine resolution satellite data.

#### *3.4.1. Distance Accumulation*

As discussed in Chapter 2, previous studies have found that manmade wildfire outbreaks were the leading cause of fire. This was why the project's focus was on surrounding roads and transmission lines. Roads were represented on maps as a line. A line feature had to be expanded so by adding a second dimension a road feature accumulated more information. A one-dimensional object can contain only information in one direction while 2D objects has length and width. Since, the majority of wildfires were triggered by human negligence then the assumption was that the road network represented a starting polygon from where a person can move. Often, camping or hiking can lead to a more relaxed behavior while under the influence of alcohol or medication. Human factors were pointed out by Ventura and Vasconcelos (2006).

Taking the previously mentioned work into account, this thesis developed a methodology to create susceptibility maps that started with importing TIGER shapefile road layer.

A buffered roads layer was derived from the TIGER/Roads shapefile that covers CA. When examining AOI this study delineated one road that passed through the AOI. Selected feature was

extracted from the shapefile through Create a Layer From selected feature option and displayed on the map. The newly created layer was projected to match the Planet data coordinate system. In the next step, the road layer was buffered with a 12 m ring around the line feature. A 12 m range was chosen after examining Planet Scope imagery and measuring the width of the road with the measurement tool. The width was ranging from 18 m to 22 m based on 3 m pixel resolution. Once the buffer was created then a layer was brought to a Model-builder where it was processed with the Distance Accumulation tool. A tool calculated the distance encountered by a person or variable that moved through the system.

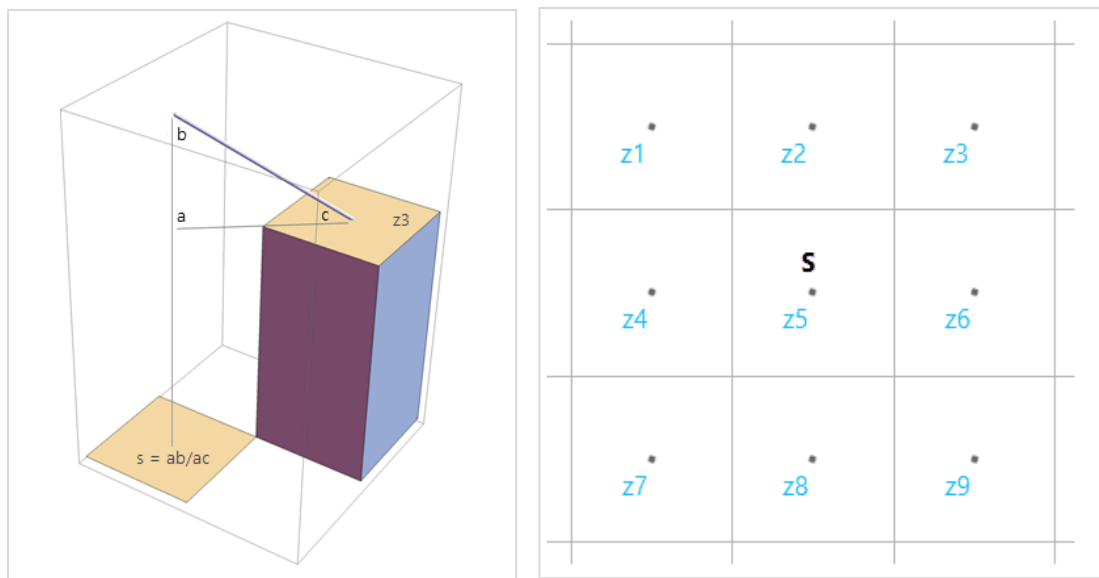


Figure 6. 3D (left) and 2D (right) models for Eikon equation.

The algorithm that calculated surface cost approximated the height from the center of each cell where it used the slope from the input cost raster layer, Slope layer. The slope **S** from the input cost surface was evaluated as the slope of the hypotenuse of the triangle abc (Figure 6).

Finding the shortest or fastest distance, or least-cost path, impact, time surface is often explored in GIS. This problem has been observed in this study in the context of a person moving through a terrain with the original starting line being centered at the buffered road layer.

Selecting the most appropriate route or the most appropriate impact surface was difficult because each additional segment of the path was not independent from other line segments (Goodchild 1977). The algorithm was governed by the Eikonal equation (4). This method has been tested in detail and insofar it has been shown that second order Gauss-Seidel iteration was sufficient for distance function in n-dimensions.

$$(4) \quad |\nabla u(x)| = f(x), x \in R^n$$

To simplify, a person making an impact can move in vertical, horizontal, and diagonal directions. Imitating Queen's movement in chess that can be simplified in 2D surface as shown in Figure 5. However, the dynamic nature of the movement, as previously mentioned, interdependence between line segments and vertical factors complicated solutions. Further, the project added DEM data and synthesized DEM derivatives with the Distance Accumulation layer.

### 3.4.2. *Electric Lines*

The Bobcat fire was attributed to electric lines and tree branches touching them. This happened during the extreme Santa Ana period where the high winds were blowing hot dry air from the desert.

The electric lines shapefile was acquired from Southern California Edison Power Site Search Tool. In multistep process electric transmission lines were selected with a selection tool thus the extent fell within AOI. This approach buffered the extracted layer with a 5m buffer hence adding width or second dimension. A 5-meter buffer choice was done after examining Google Earth Pro imagery for the AOI. The width approximation from tree branches to a cable was estimated with a measuring tool.

Further, this project converted a vector layer to raster with the Feature to Raster tool keeping the cell size at 3m. After rasterization was completed the layer was Reclassified as 1.

To connect different layers, the NDVI layer from Planet data was also reclassified with a previously mentioned tool. The reclassification tool assigned 0 as not-susceptible to the NDVI layer with a range from 75 to 150 and from 150 to 189 to 1 or susceptible. In this way, both layers could be combined with the Raster Calculator (Spatial Analysis Tool).

The output layer was then reclassified manually to switch results and assign 0 to not-susceptible and 1 to susceptible areas.

### *3.4.3. DEM Layer Processing*

Data quality has a substantial influence on analysis and pre-processing, cleaning, and refining datasets are necessary steps before any analysis takes place. Most DEM layers contain either spurious pits or peaks that are contained within pixel arrays and this is just a physical limitation of instruments. Since DEM datasets were produced by synthetic aperture radar SAR, then naturally due to terrain's complexity there will be pixels that contain erroneous data. The literature explanation (Bolstad 2017) was that a possible issue arises from spurious pits that are located within the DEM layer. Pits are raster cells that have lower value than surrounding cells. The downside of running the tool was that the output raster can require up to four times more storage space than the original raster. In the tool, settings z-score controlled the range between the depth of a sink and the pour point and determined which sinks will be filled and which will remain unfilled.

Although, the model used a Fill Tool to clean from pits but the efficiency was not hundred percent. In addition, a future work can add Sink tool before Fill tool in their analysis

since the output identifies the depth in raster data. Once that was solved then setting z-score was more straightforward.

Completeness	Logical Consistency	Temporal quality	Coordinate System	PCS
complete	logic	srctime	NAD 83	UTM 11N

Description of Dataset	Usage	Source of data	Metadata (Conform)
Raster data 1 arc second -30m	National elevation dataset	USGS - Elevation Products	<a href="http://FGDC.gov">FGDC.gov</a>

Table 4. DEM Data Description.

#### 3.4.4. Creating Hill-shade and Slope Layers

Hill shade tool simulated the Sun’s position above the terrain and shows the reflectance of the surface. Since the simulation was done by algorithm we can expect that bias within the algorithm will propel throughout the analysis.

Actually, the hill shade surface represents a discrete object in a raster data set. Because we see the snapshot in time. The shade in reality moves across the surface as the Sun’s position is changing over the sky. Hence, we have a snapshot based on the chosen incoming sun beam and reflection (Zhang, Li, and She 2019). The reflecting light of a pixel cell depends on incidence angle.

Hill-shade tool processing was adjusted according to Planet satellite data, hence the azimuth and altitude angles, sun’s relative position, are set to 142 and 62 degrees. These metrics were obtained from Planet satellite info section which corresponds to flyover time of the images taken on 24 August, 2020 above the Angeles National Forest (ANF). The same approach was used to adjust the sun's relative position for September 6 2020.

Further, Slope, and Hill-shade were processed using the Rescale Function Tool, Figure 7. For each layer a specific transformation function is applied. Slope and Hill-shade layers are rescaled with Large transformation function indicating that the larger input values have higher preference. Salis (Sails et al. 2014; Alan et al. 2011) used a similar approach where the slope, aspect, and elevation layer were combined with vegetation cover.

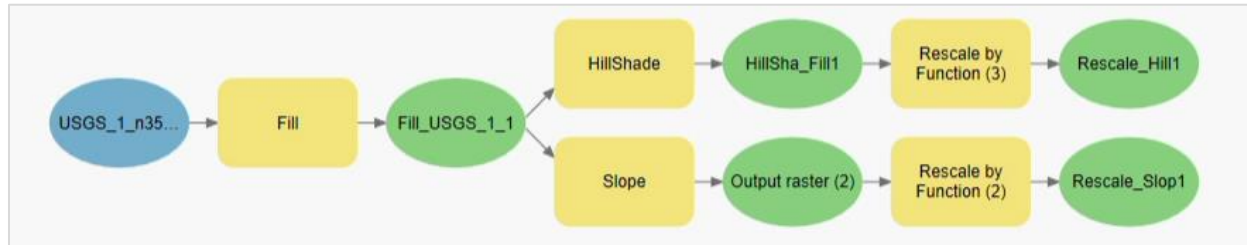


Figure 7. Model-builder schema for DEM processing.

#### 3.4.5. NDVI Layer from PlanetScope Data

PlanetScope is part of Planet’s satellite constellation and offers almost daily visitation capturing a swath of 24 km by 8 km. The onboard sensor covered four bands, and out of four three were RGB and one was in NIR (B 4 band at 0.733-0.748(μ)). Combination of bands 3 and 4 created NDVI indices, equation (5). NDVI has been used as an indicator for drought and vegetation density. This project chose two dates for susceptibility assessment, 08/24/20 and 09/06/20. Each image was downloaded from the Planet data webpage. Once the images were downloaded then using the merge raster function all images were stitched together with the overlap method set to mean. From here the NDVI tool, from raster functions, created the NDVI layer by selecting channels 3 and 4 which corresponded to red and IR wavelengths. In the first round this method produced standard scientific pixel value output that ranges from -1 to 1. However, due to complications with Rescale by function tool that arose from parameterization issues this project switched to 0-200-pixel range. Before continuing with this range, the analysis compared the results from both, scientific and default equation output. The comparison

confirmed that in both cases higher values were indicators of green vegetation. For scientific output a zero means no vegetation and close to +1 (0.8 - 0.9) indicates high density of green leaves. Which was related to the default equation in a way that the values from 150 to 179 were the indicators of green areas. The equation 5 shows the default equation for NDVI calculation in ArcGIS Pro environment.

$$(5) \quad NDVI = ((IR - R)/(IR + R)) * 100 + 100$$

#### *3.4.6. Susceptibility Synthesis*

This project developed two approaches for pre-fire susceptibility assessment. The first approach was weighted classification and the second was hard classification. The first approach was run with the Model-builder tool where all the layers were included and executed, as shown in Figure 8. However, after multiple re-runs the tool has started failing or taking too much time to complete geoprocessing.

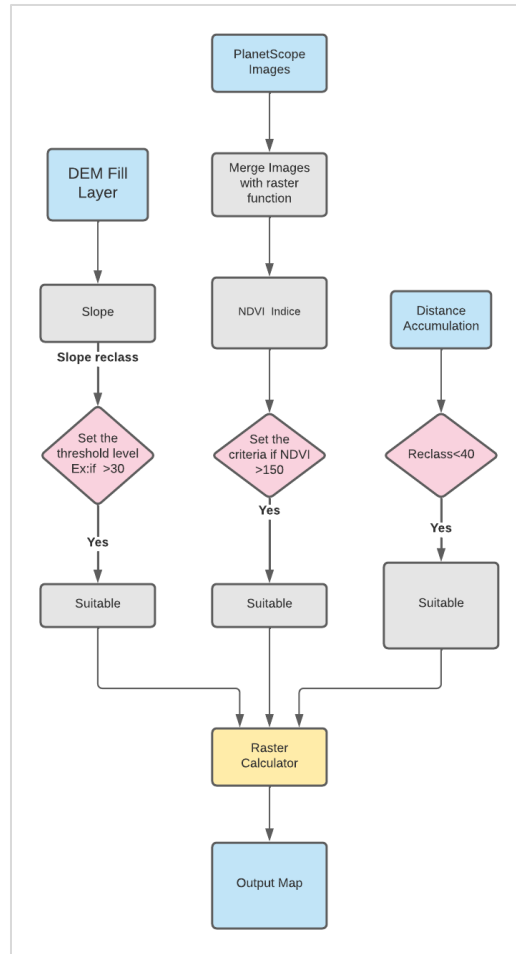
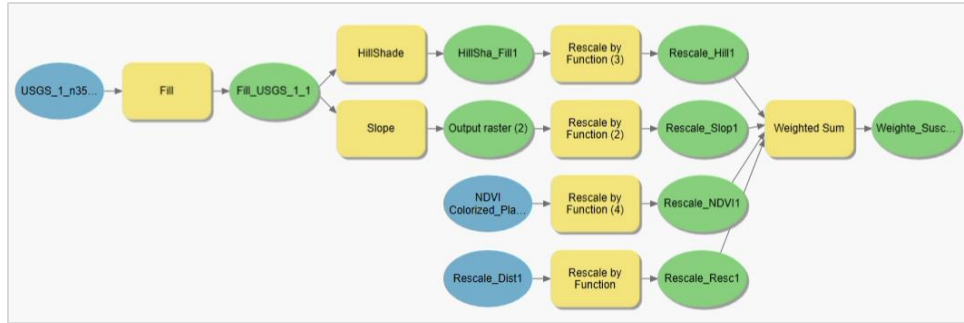


Figure 8. Weighted classification (top) and hard classification (bottom) susceptibility analysis models.

To work around this issue this research broke down the Model-builder into smaller components and ran the tool with fewer steps in Model-BUILDER and it also used the Notebook Python environment.

## Chapter 4 Regional and Local Results

In this chapter results were presented in the following order: raster predictive scenario (Figure 9), regional results from indices analysis, susceptibility scenario - local extent, and synthesizing and comparing different extents and resolutions.

### 4.1. Raster Predictive Scenario

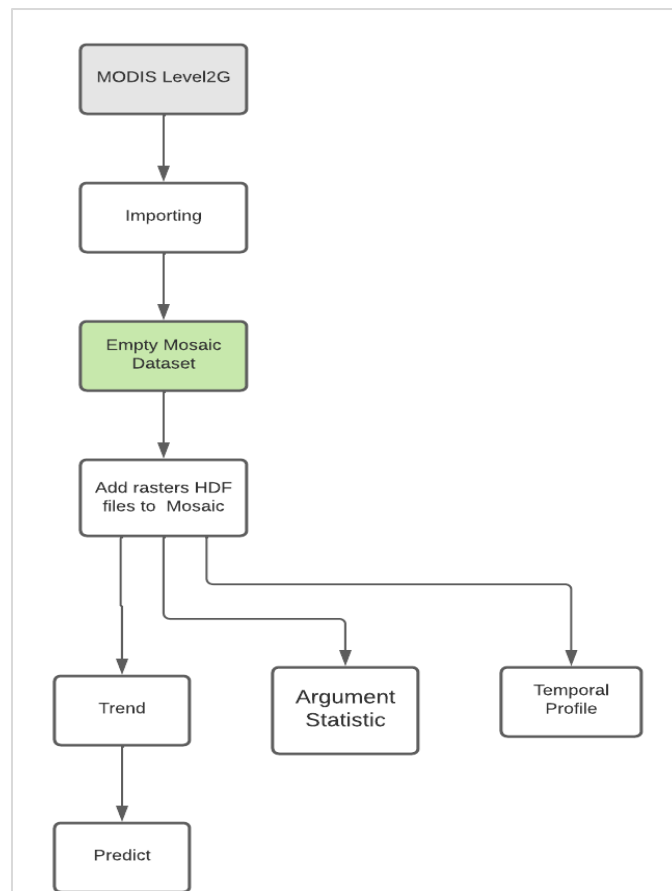
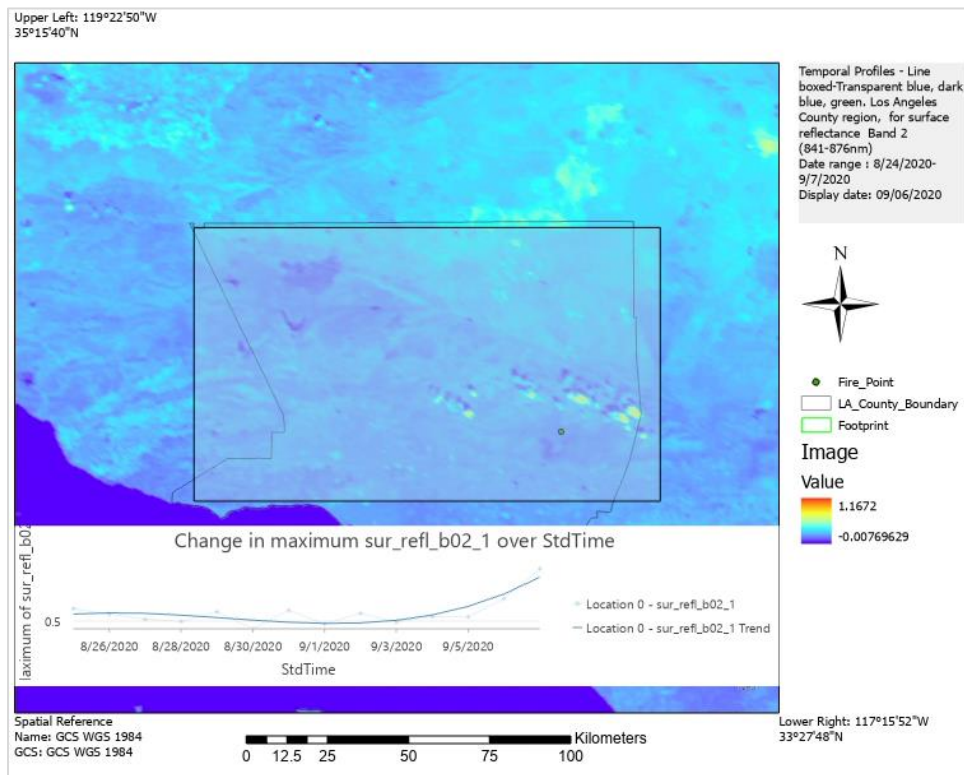


Figure 9. MODIS Multidimensional Workflow.

#### 4.1.1. Temporal Profile

A basic visual inspection of surface reflectance with the MODIS instrument was performed with a temporal profile tool in ArcGIS Pro. The temporal profile tool is part of a multidimensional data management package that allows big data utilization. A temporal profile was created for (Band 2) NIR, (Band 6) SWIR1, and (Band 7) SWIR2. The date range was set between 08/24/2020- 09/07/2020. The first step was to create a set up parameters in the chart property tab section. In the Chart property settings this approach chose a multi-location with one variable tab and trend line was set to Harmonic trend line. For the Spatial and temporal aggregation project chose maximum values. While the time interval size was set to Days (Figure 10.1-3).



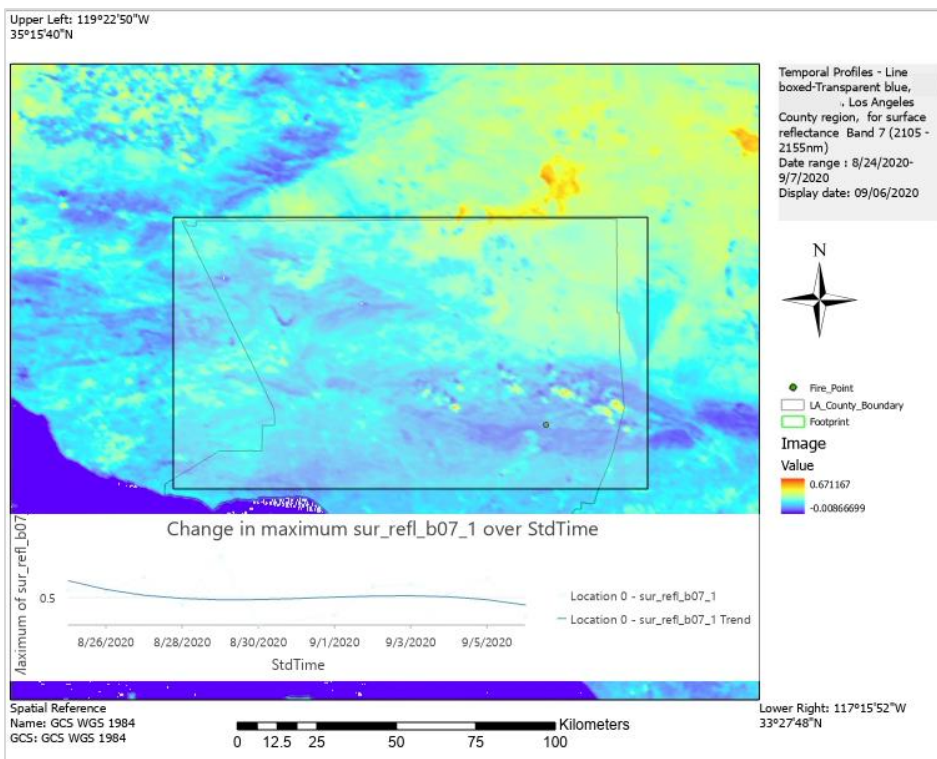
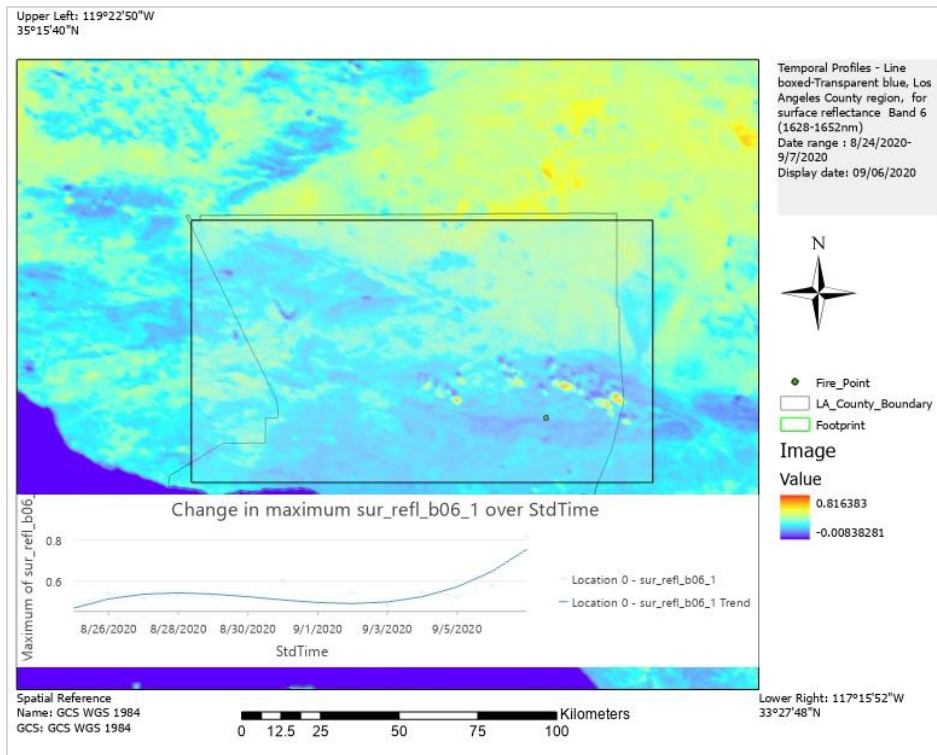
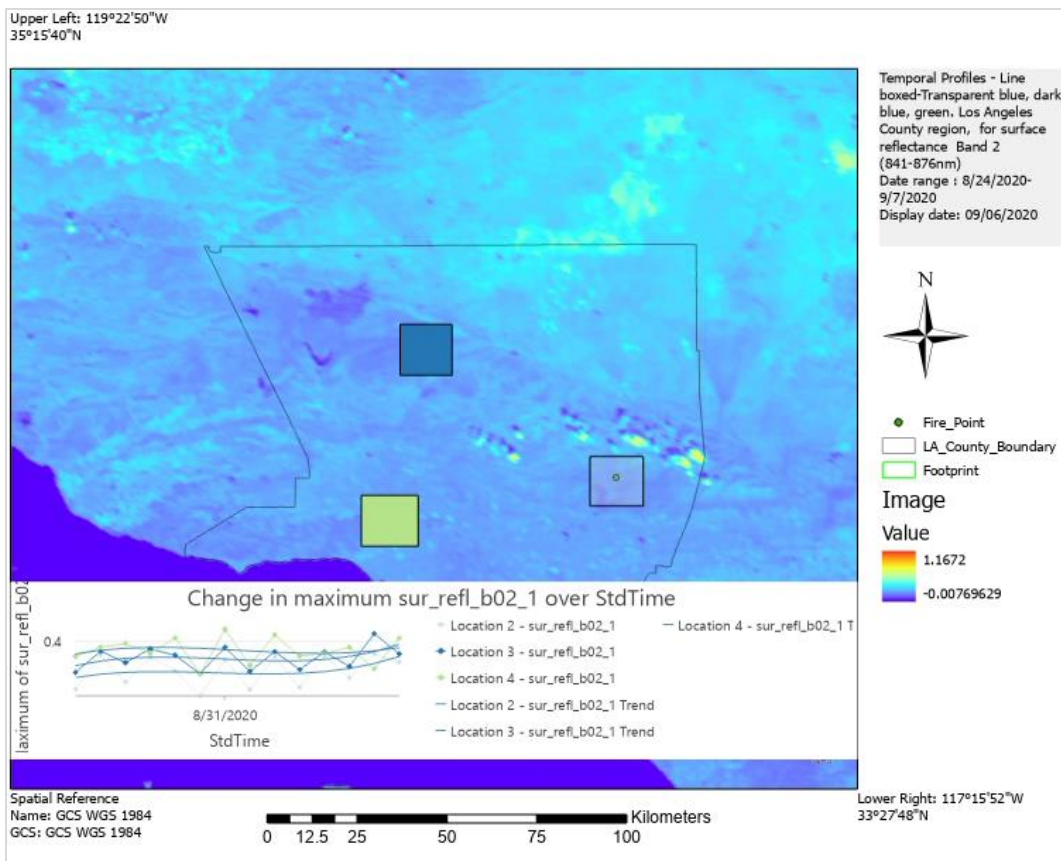


Figure 10 (1-3). Temporal profile for NIR (top), SWIR1(middle), and SWIR2 (bottom) channels, Line Boxed Extent.

Figures 10 (1-3) and 11 (1-3) the chart properties are displayed at the upper corner of the main map frame. The central section of the map has Los Angeles county delineated with a pale gray line while the rectangular bounding box represents the sampling aerial coverage for surface reflectance. It is worth pointing out that the sampling box in Figure 10 (1-3) was chosen carefully in order to avoid reflectance over the ocean surface. The surface reflectance over the ocean could skew the average results, because of water’s ability to absorb IR and NIR (Campbell and Wynne 2011).



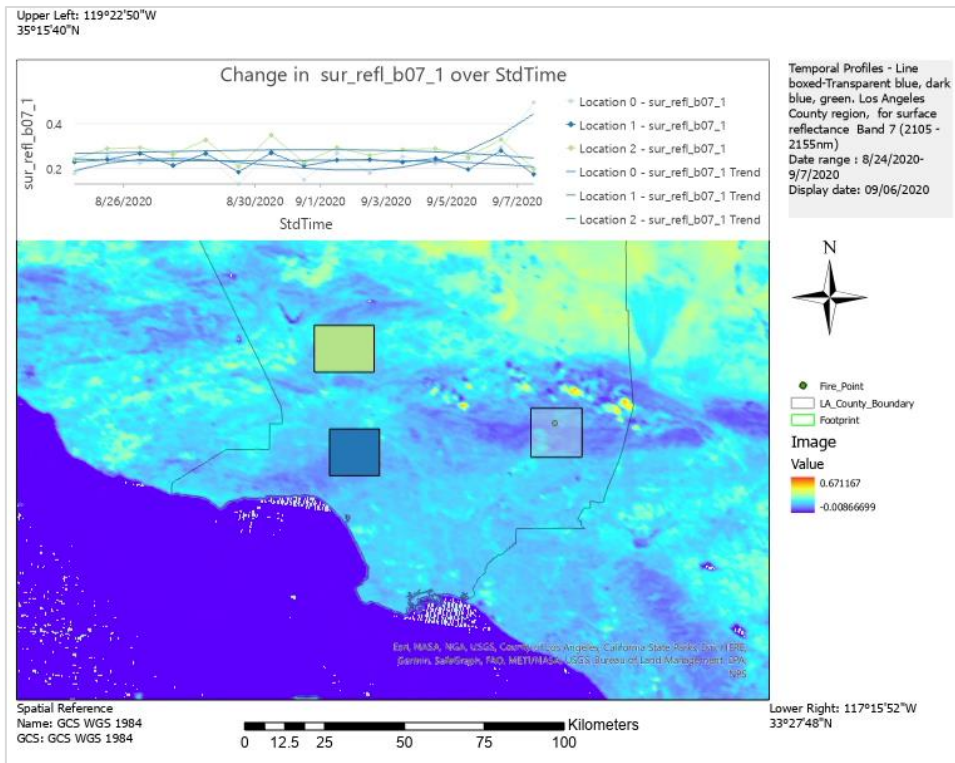
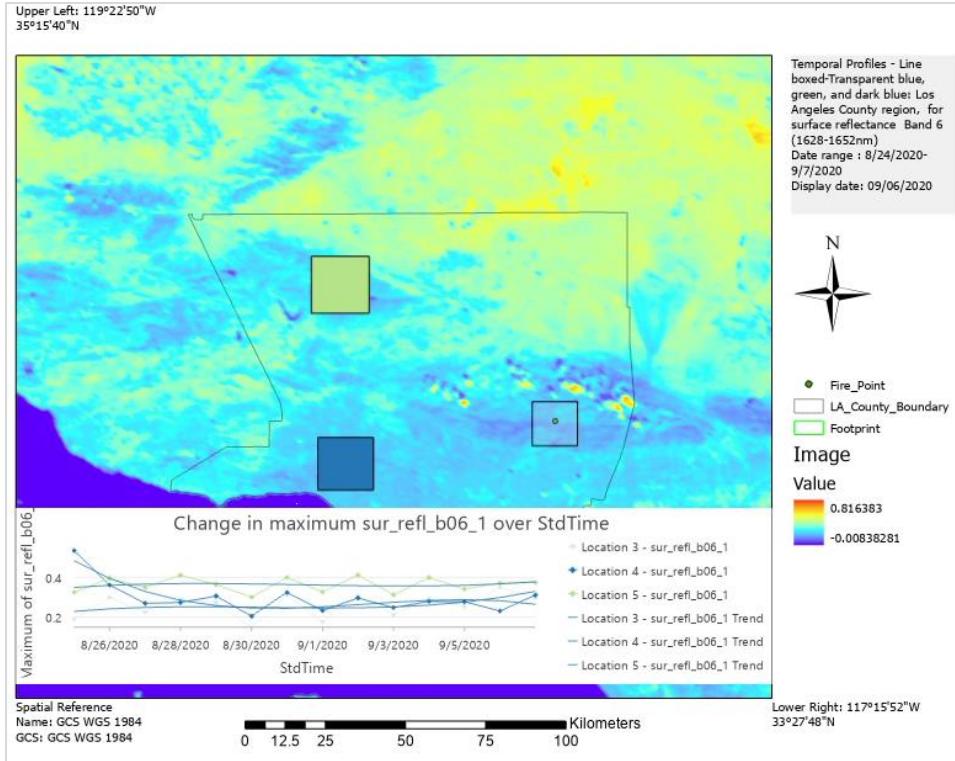


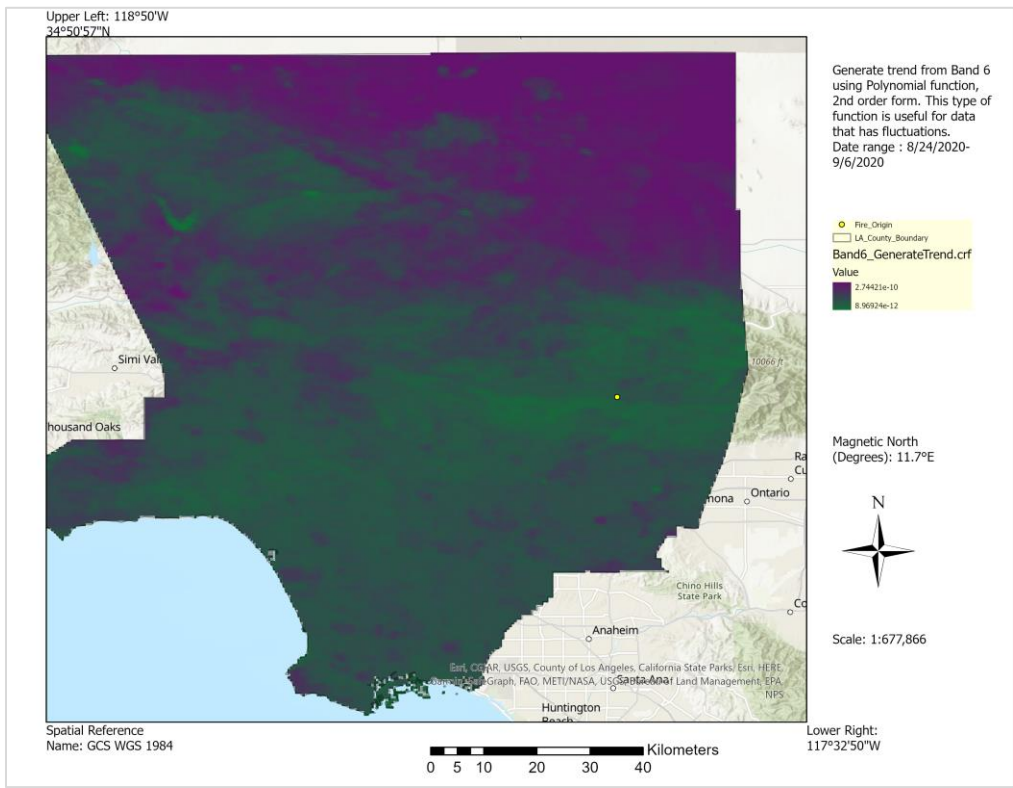
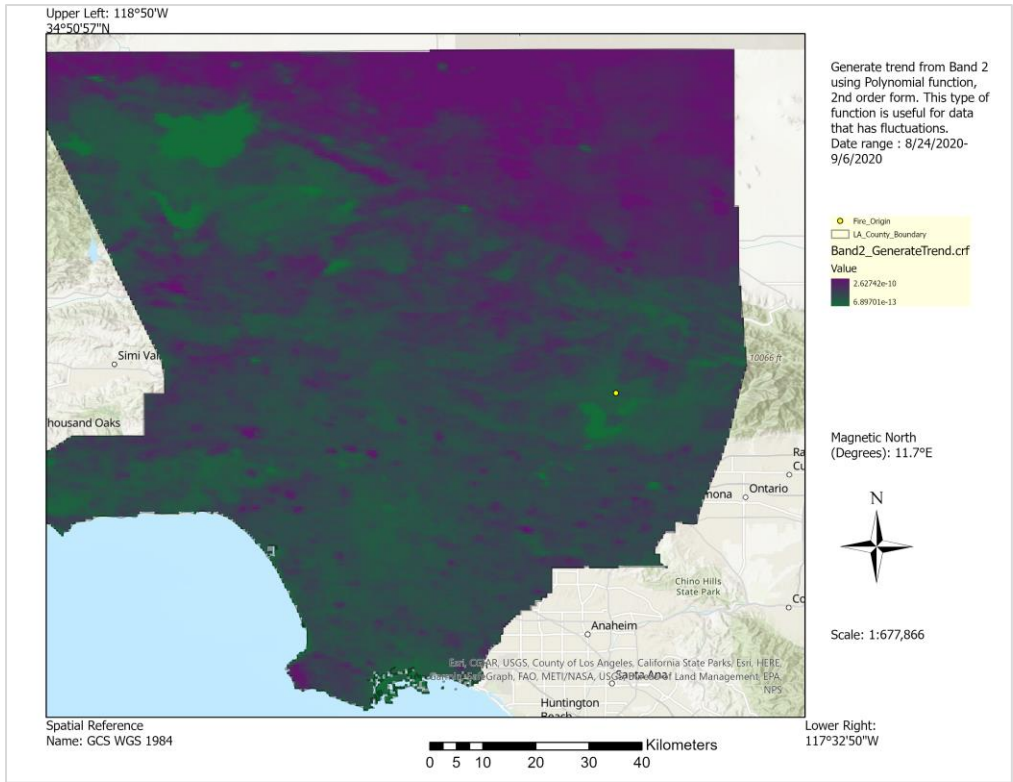
Figure 11 (1-3) Temporal profiles for NIR, SWIR1, and SWIR2 bands, Line Boxed Extent-Transparent blue, dark blue, and green.

Figure 11 (1-3) showed finer scale with three sampling locations for each band. Of special interest is AOI where the fire erupted. In the chart property tab three boxes were drawn for the purpose of comparing SR readings from each area. Transparent blue box on top of AOI and two more areas with approximately the same spatial extent are displayed in Figures 11 (1-3). Also, three charts for each band are displayed on top of the main map frame. Three sampling boxes, Figure 10, did not reveal significant changes in surface reflectance on the observed temporal range. A spike visible on chart surface readings was detected on September 7 which was one day after fire was ignited.

#### *4.1.2. Trend*

Temporal profile tool enables a fast display of HDF data. However, the trend within multidimensional data was not clearly visible from the temporal profile. The Generate Trend Raster tool created a multidimensional raster that estimated the trend for each pixel over the entire time series. For a more precise estimate, this project adjusted the type of trend to polynomial to account for changes that happen throughout the two-week period between each day in a fluctuation pattern. This choice considered the short-term changes in surface reflectance temperature.

Map displays pixel value changes on the right in the legend box, Figure 12. Values exhibit high accuracy, between 10 and 12 decimal places. Thus, the LZ77 compression type was kept for storing raster output. Accuracy requirement increased processing time and storage volume.



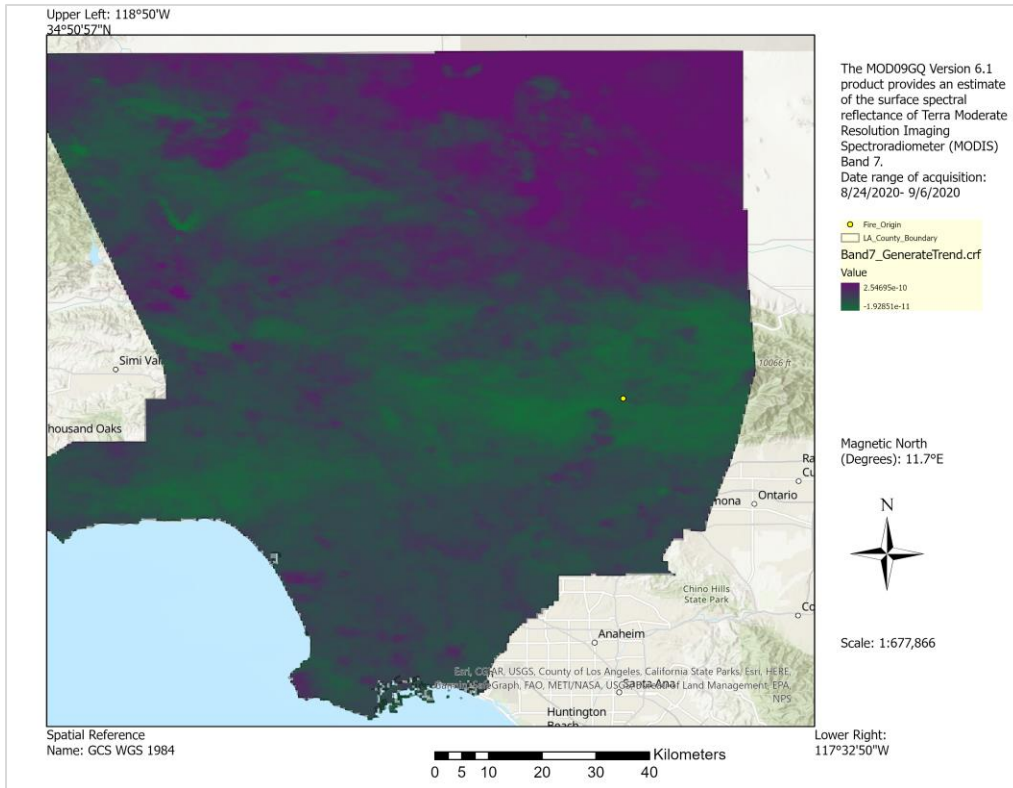
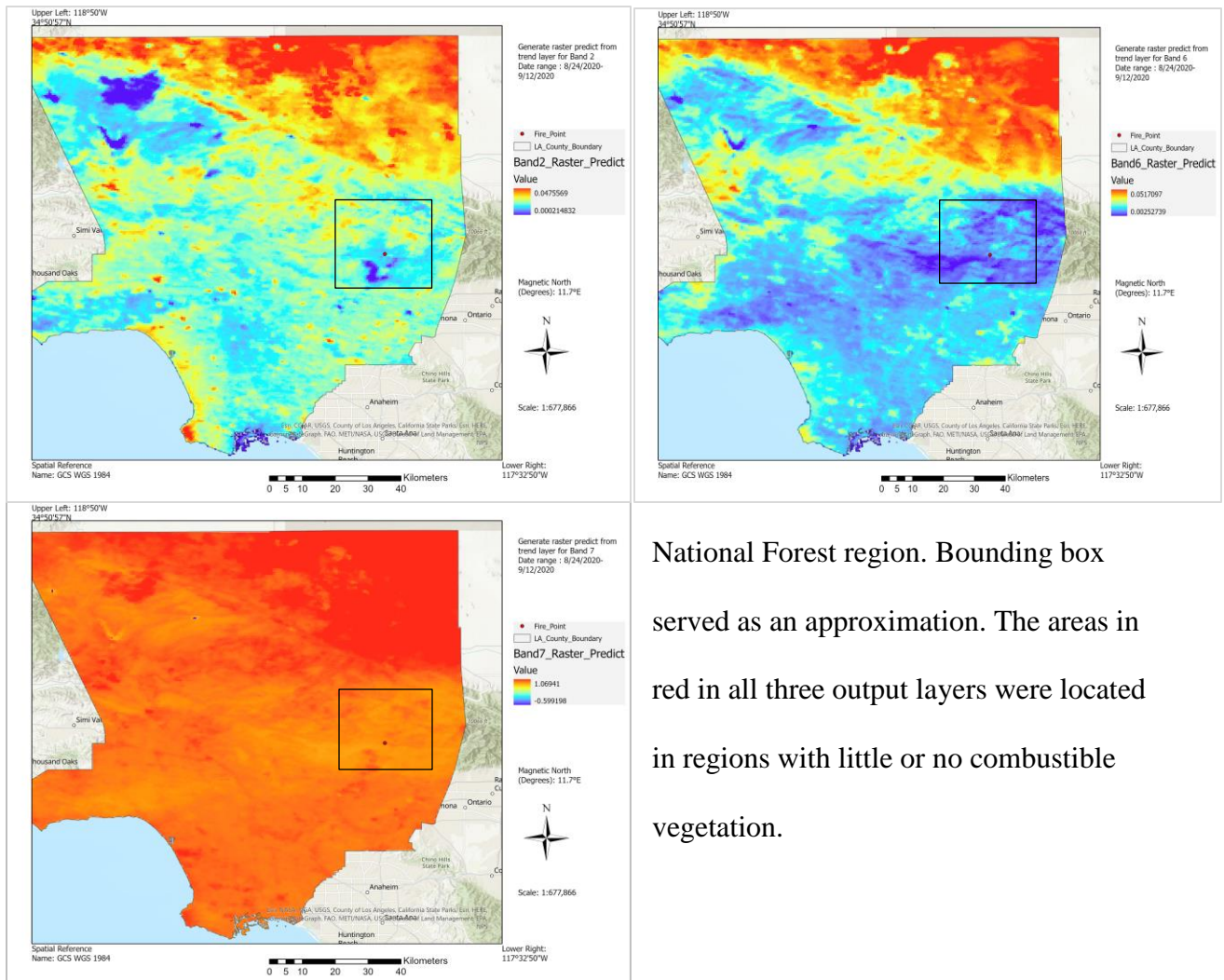


Figure 12 (1-3). Trend Analysis Bands 2,6 and 7.

The output multidimensional raster in Figure 12 indicated the direction of change in surface temperature values between 8/24/20 and 9/06/20. Small positive values were present, which represent the slope of change in each pixel. If negative values were present that would indicate a positive slope change in pixel values. Output CRF layers indicated that the change in direction was slightly positive and for the observed date range this approach did not detect an area with substantial pixel slope change.

### 4.1.3. Raster Predictive Model

Figure 13(1-3) the Predict Using Trend Raster tool created a multidimensional raster that predicted new hypothetical future surface temperature values based on the trend raster. As discussed in chapter 3, temporal range was set from 08/24/2020 - 09/12/2020. Thus, the tool used a two-week trend to predict one week in the future. Same as in Trend analysis, the values displayed on map legend indicated the slope of pixel change. Results from Predict analysis suggested that there was a fluctuation in future surface temperature in the Angeles



National Forest region. Bounding box served as an approximation. The areas in red in all three output layers were located in regions with little or no combustible vegetation.

Figure 13 (1-3). Predict Raster layers. Channels 2,6, and 7 (bounding box ~ Angeles National Forest)

#### 4.1.4. Argument Statistic

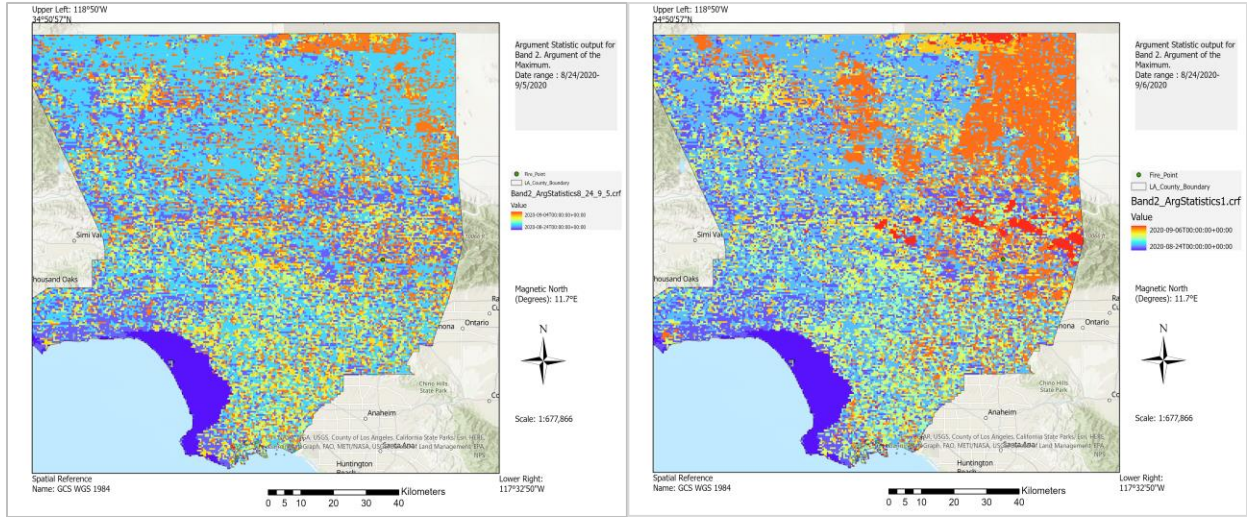


Figure 14. Argument Statistic map for Band 2, Maximum values: Temporal range (08/24/20 -09/05/2020; left) and (08/24/2020 – 09/06/2020: right).

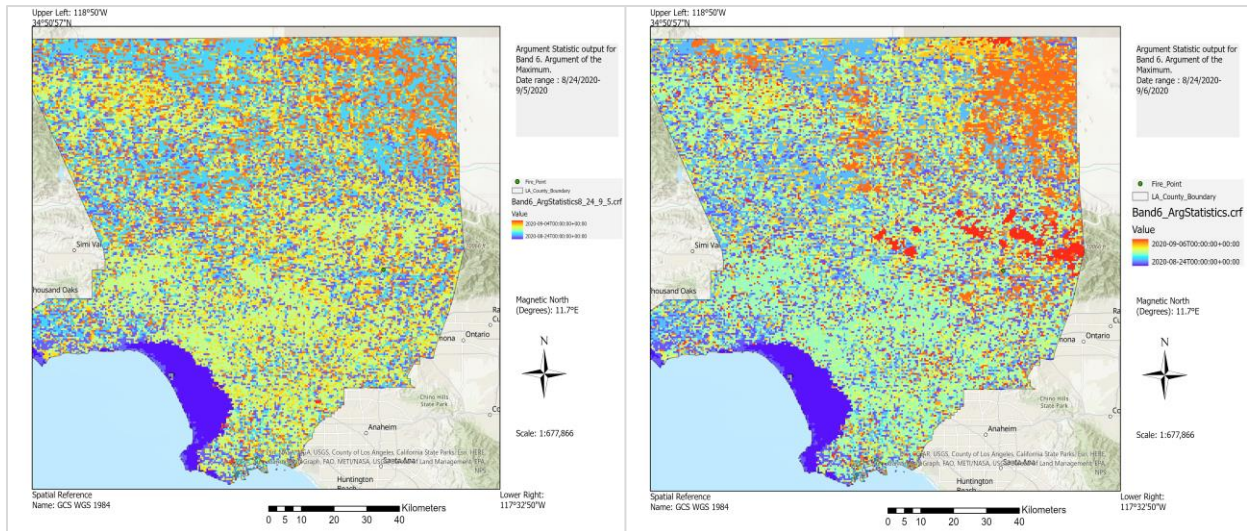


Figure 15. Argument Statistic map for Band 6, Maximum values: Temporal range (08/24/20 -09/05/2020; left) and (08/24/2020 – 09/06/2020: right).

This step of the project measured the duration of exposure at which each pixel reached the maximum value during the two-week period. In Figures 14-16 two maps for two different time ranges are displayed, as specified. Shortening analysis for one day was done after the first round of analysis was performed for 08/24-09/06 date range. However, after visual inspection the assessment concluded that cloud cover affects results and shifted the pixel values towards maximum. Clouds were located near the fire outbreak region. Since water vapor emits radiation from the top of the clouds then the surface reflectance was not readable from satellites.

Therefore, assessment shortened analysis for one day by using cloud free imagery.

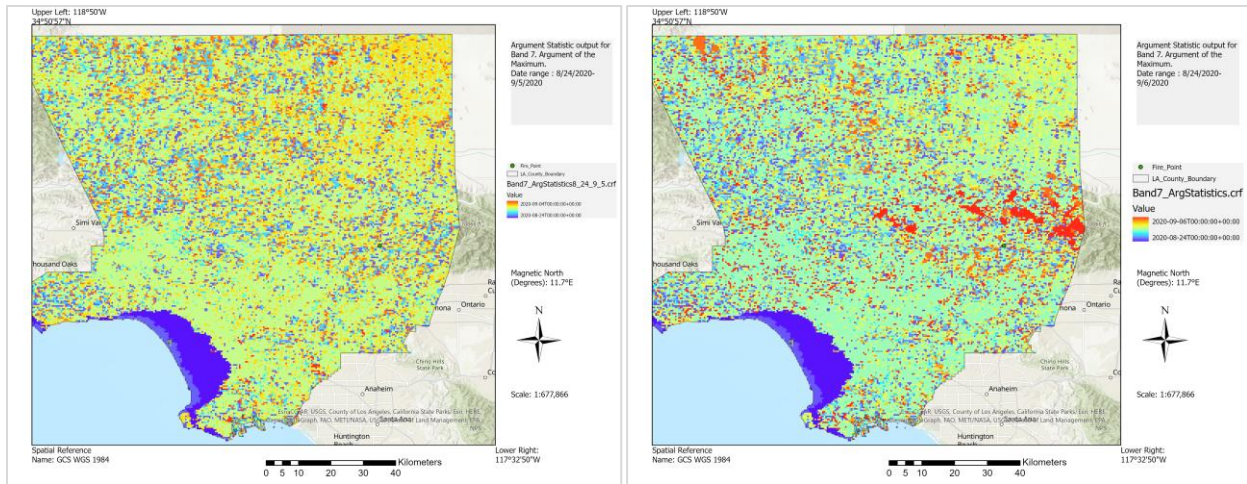


Figure 16. Argument Statistic map for Band 7, Maximum values: Temporal range (08/24/20 -09/05/2020; left) and (08/24/2020 – 09/06/2020: right).

## 4.2. Regional results from indices analysis

For the time range between August 24, 2020, and September 6, 2020 IDRISI created a NMDI and NDWI raster index for each day. The index creation was fairly easy and each raster creation took 4-7 minutes to create. Further, each image was normalized manually where in Layer Properties the classification schema was set to equal intervals with stretch type, number of classes 256. Also, the display setting values as a part of manual normalization were set from 0 and 1.

Contrary to NMDI index that required raster calculator NDWI was created with image processing VEGINDEX display that was already set up for processing NDWI. After each image was created the pixel values were set to scientific scale from -1 to 1.

*4.2.1. PCA Analysis (8/24/2020 and 9/06/2020 Images)*

Before the aforementioned NMDI analysis took place, this project tested the viability of data saving statistical analysis. Principal Component Analysis was performed on channels 2,6, and 7 for two dates, 08/24/2020 and 09/06/2020 with IDRISI TerrSet software.

Four output tables from PCA analysis created new uncorrelated variables from a data set. Since the governing variable was temperature in multispectral data which makes Bands 2,6, and 7 highly correlated. The TerrSet has two PCA methods: the forward t-mode and s-mode. In the t-mode images are analyzed as a temporal change while in the s-mode images are processed as spatial variables. This project used the t-mode process. The PCA process included rotation and translation of the band's axes while at the same time it produced the same number of new bands that were orthogonal to each other in data space.

T-MODE VAR/COVAR	B2 8/24	B6 8/24	B7 8/24	B2 9/6	B6 9/6	B7 9/6
B2 8/24/20	2334505	1694940	1553376	39416.56	28009.06	-14695.8
B6 8/24/20	1694940	1947262	1776244	242522.5	460756.6	487760.9
B7 8/24/20	1553376	1776244	5473963	384969.9	661730.9	848812.5
B2 9/6/20	39416.56	242522.5	384969.9	1441494	1511751	1495765
B6 9/6/20	28009.06	460756.6	661730.9	1511751	1989063	1903853
B7 9/6/20	-14695.8	487760.9	848812.5	1495765	1903853	6312743

T-MODE COR. MATRIX	B2 8/24	B6 8/24	B7 8/24	B2 9/6	B6 9/6	B7 9/6
B2 8/24	1	0.794959	0.434538	0.021487	0.012998	-0.00383
B6 8/24	0.794959	1	0.544051	0.144755	0.234118	0.139119
B7 8/24	0.434538	0.544051	1	0.137047	0.200542	0.144395
B2 9/6	0.021487	0.144755	0.137047	1	0.89279	0.495847
B6 9/6	0.012998	0.234118	0.200542	0.89279	1	0.537279
B7 9/6	-0.00383	0.139119	0.144395	0.495847	0.537279	1
T-MODE COMPONENT	C 1	C 2	C 3	C 4	C 5	C 6
% VAR.	44.29467	31.91338	11.182	9.788297	2.078551	0.743103
T-MODE EIGENVAL.	8637032	6222799	2180381	1908623	405297.3	144897.9
T-MODE EIGENVEC. 1	0.20457	-0.3768	0.657763	0.037474	-0.58182	-0.2088
T-MODE EIGENVEC. 2	0.271467	-0.30762	0.47323	-0.05961	0.731383	0.263166
T-MODE EIGENVEC. 3	0.528166	-0.60981	-0.5804	0.085736	-0.07043	0.001191
T-MODE EIGENVEC. 4	0.244051	0.170338	-0.00279	-0.57782	-0.31335	0.692354
T-MODE EIGENVEC. 5	0.318657	0.186913	-0.02323	-0.65749	0.151541	-0.63854
T-MODE EIGENVEC. 6	0.666629	0.57234	0.077411	0.47067	-0.02122	0.007724

T-MODE LOADING	C 1	C 2	C 3	C 4	C 5	C 6
B2 8/24	0.393484	-0.61519	0.635679	0.033884	-0.24243	-0.05202
B6 8/24	0.571725	-0.54991	0.500757	-0.05901	0.333672	0.071787
B7 8/24	0.663441	-0.65018	-0.3663	0.050626	-0.01916	0.000194
B2 9/6	0.597388	0.353914	-0.00344	-0.66488	-0.16615	0.219509
B6 9/6	0.66402	0.330604	-0.02432	-0.64405	-0.068406	-0.17234
B7 9/6	0.779753	0.568248	0.045495	0.258802	-0.00538	0.00117

Table 5. Output from PCA Analysis Bands [2,6,7] Dates: 08/24/2020 and 09/06/2020.

The first table shows the variability of the bands and how bands relate to each other. On the second table PCA displays correlation matrix. A correlation matrix display coefficient which provides the maximum knowledge that can be transferred by any single band created by linear combinations of original bands. On the side note, calculation of the previously mentioned coefficients is better described in advanced statistical publications (Gould 1967).

The third table shows transformed bands. Each band was formed from a linear combination of original bands. Bands 2 and 6 account for about 75 % of total data variation. While Bands 2,6, and 7 account for about 86 % of total data variation. The result of declination in data content is visible in Figure 17. Where PCA components 1,2,3, and 4 are compared side by side. The remnants of the noise in the system from the atmospheric scattering and topo features were contributing to image brightness as well. Previous publications reported over 90% in data variation from one channel and when adding one more channel data variation often achieved 95-98%. Therefore, this thesis chose to abandon PCA methods for data savings approach.

Results from PCA suggest that substantial information would be lost if the project relied only on PCA components.

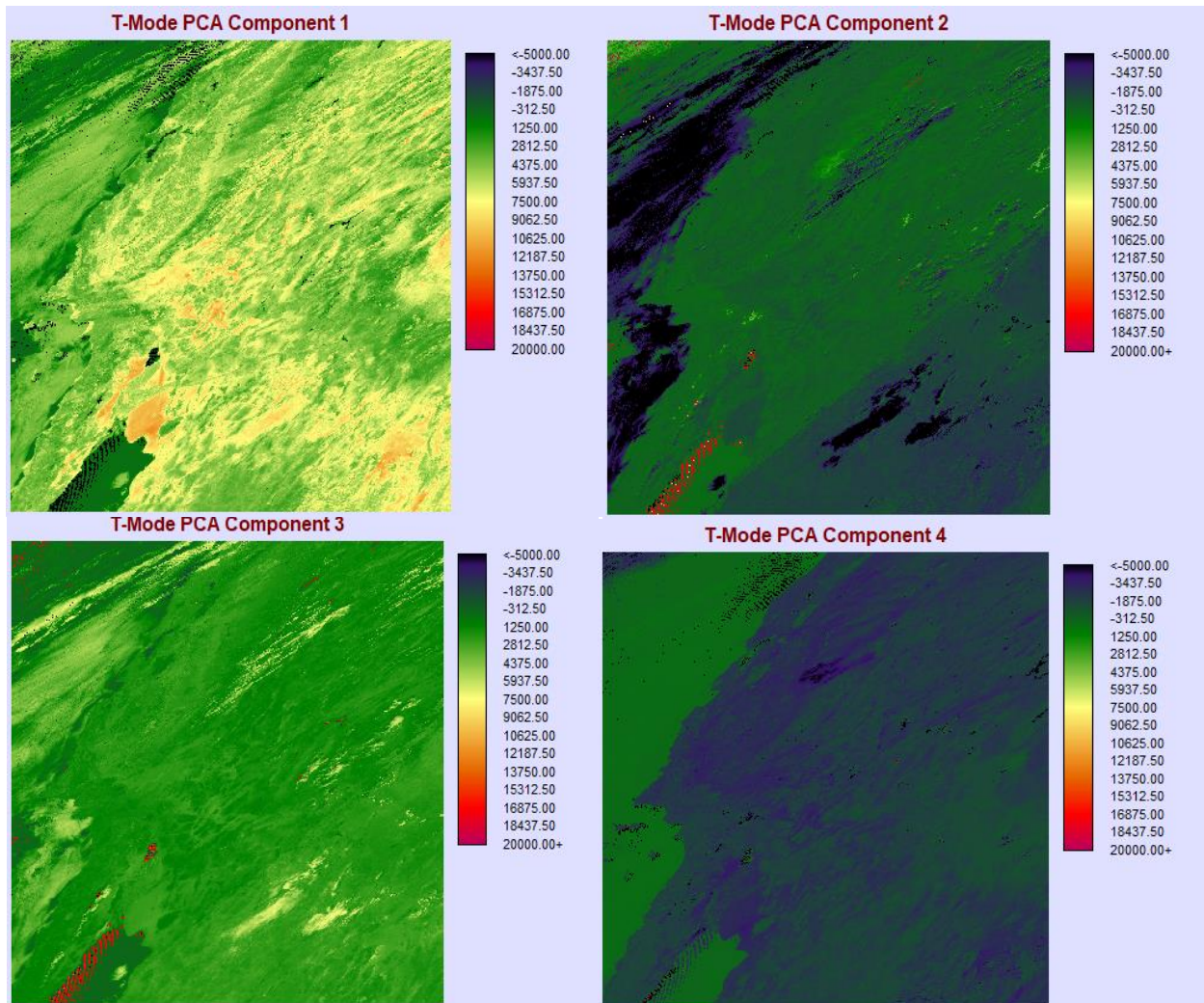


Figure 17. PCA Components 1,2,3, and 4. These images displays four out of six components for the images described in table.

#### 4.2.2. NMDI and NDWI Results

Figure 18 the Southern California extent is visible on the left. Los Angeles County is delineated with the Los Angeles County shapefile in black and on the right Los Angeles County region is overlaid with the road network. Further this scenario zoomed in to the ANF extent where the fire outbreak occurred, bottom image. At this spatial extent and pixel resolution there is apparent limitation in delineating sufficiently small fire susceptible areas. In addition, at this pixel resolution vegetation and soil in immediate fire origin proximity did not experience water

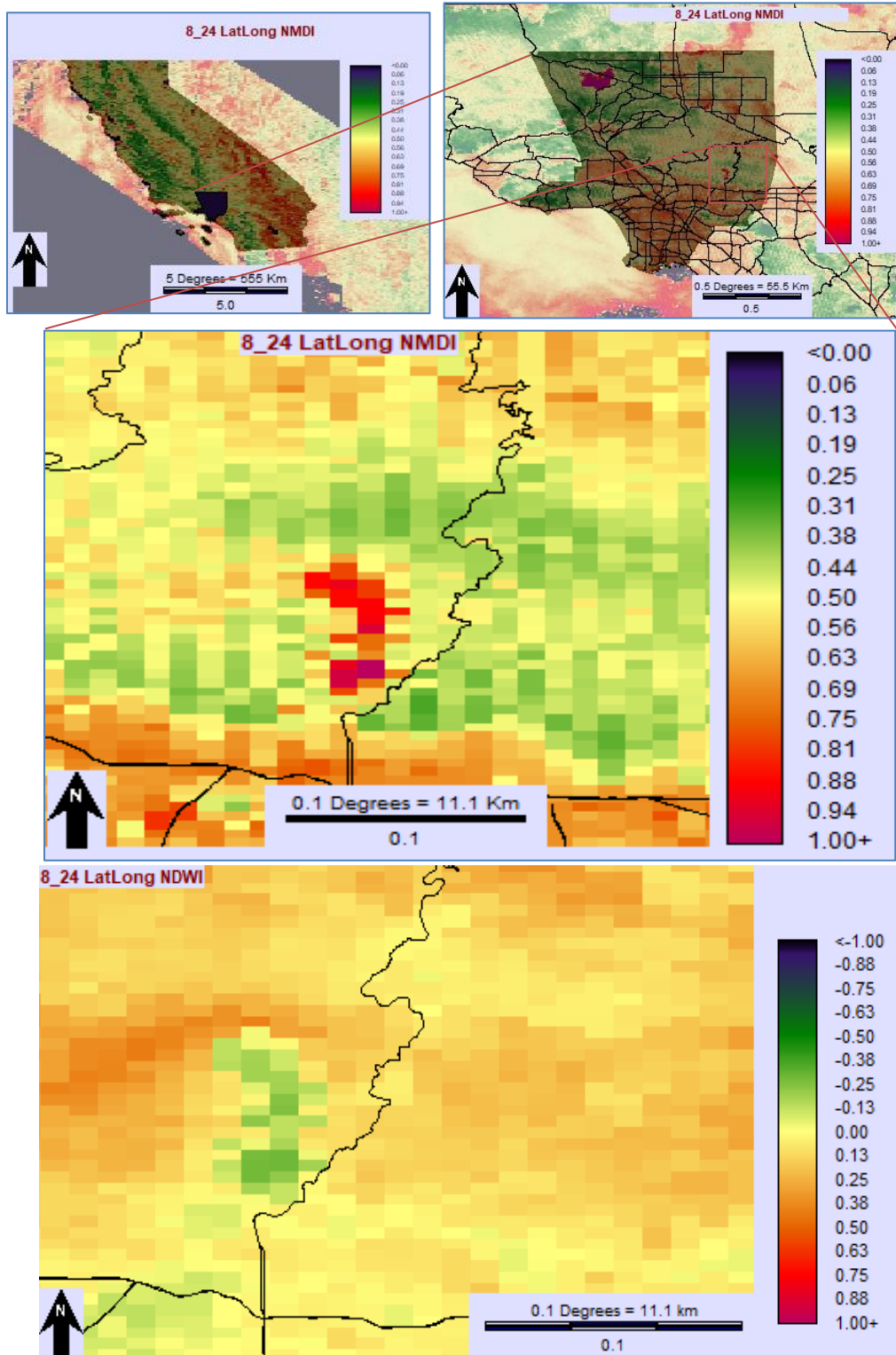


Figure 18 (1-4). NMDI Results for three spatial extents; Southern California, top left, Los Angeles County, top right, and Angeles National Forest, bottom middle. NDWI results for Angeles National Forest extent, bottom. (Acquisition date 08/24/2020).

stress that could flag this area as hazardous. In the Appendix NMDI results suggested that the Southern California area was going through drought (Appendix: NMDI and NDWI Results).

This interpretation for soil and vegetation moisture, observed by Wang in 2007, ranged from 0-1 where values 0.3-0.5 indicate medium soil dryness, and 0.7-0.9 extreme dry bare soil. Similar interpretation can be drawn from NDWI time-series imagery where the dimensionless range -1 to 1 provided the information of spatial distribution water stress. High values, close to 1, indicated higher water content, areas in red. Low values, in blue, indicated low vegetation water content. Relationships are reversed for NMDI results, red indicates low while blue indicates high water content.

The spatial distribution of NDWI and NMDI anomalies, as shown in Appendix, supported the observation, as discussed in chapter 1, that the Southern California region was experiencing severe drought (Delbart et al. 2005).

### **4.3. Susceptibility Scenario**

This section summarized results from each geo-processed layer and lastly it synthesized them in the final reclassified map products. The hope of this method was that the results would encourage more focus on GIS type pre-fire assessment by responsible agencies.

#### *4.3.1. DEM Results*

Slope was weighted into the model because steep slopes are amplifying convective heating uphill thus accelerating fire propagation. Whereas on the flat terrain fire spread is slower. However, the presence of strong winds, such as Santa Ana, contributed to fire propagation on flat surfaces. Adding Hill-shade layer was necessary thus the model considered areas that were more exposed to a sun's radiative heating during the day.

### 4.3.2. Distance Accumulation (DA) Results

Figure 19 shows maps in 3D and 2D layouts. A scale change and space rotation allowed for visualization of surrounding terrain. Accessibility of the terrain in Angeles National Forest depends on slope.

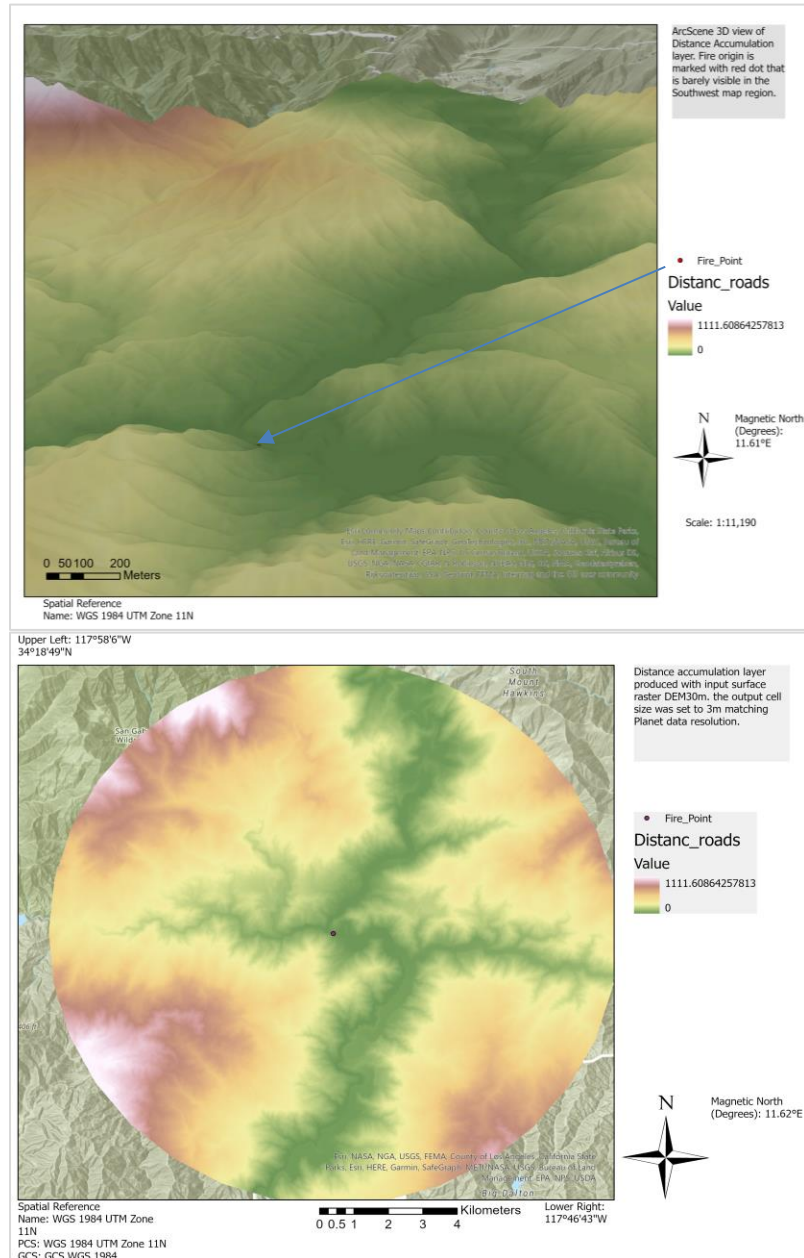


Figure 19. Distance accumulation maps (ArcView 3D, left, and 2D layout, right).

The DA tool models how easy it is for a person to move across the surface. Green areas represent areas that are accessible and close to the road. Since the starting point was the road feature, as described in chapter 3. The assumption was that hikers or random sightseeing stoppers would keep their movement close to the road. Therefore, the features that were classified with orange to red to white were deemed as less prone to human impact.

#### 4.3.3. NDVI Results

Figure 20 shows two maps with NDVI results for two different dates. The stretch type for pixel values shows a slight decline in NDVI values for September 6, 2020 when compared to August 24, 2020. This drop in healthy green vegetation volume can be attributed to continuously drying

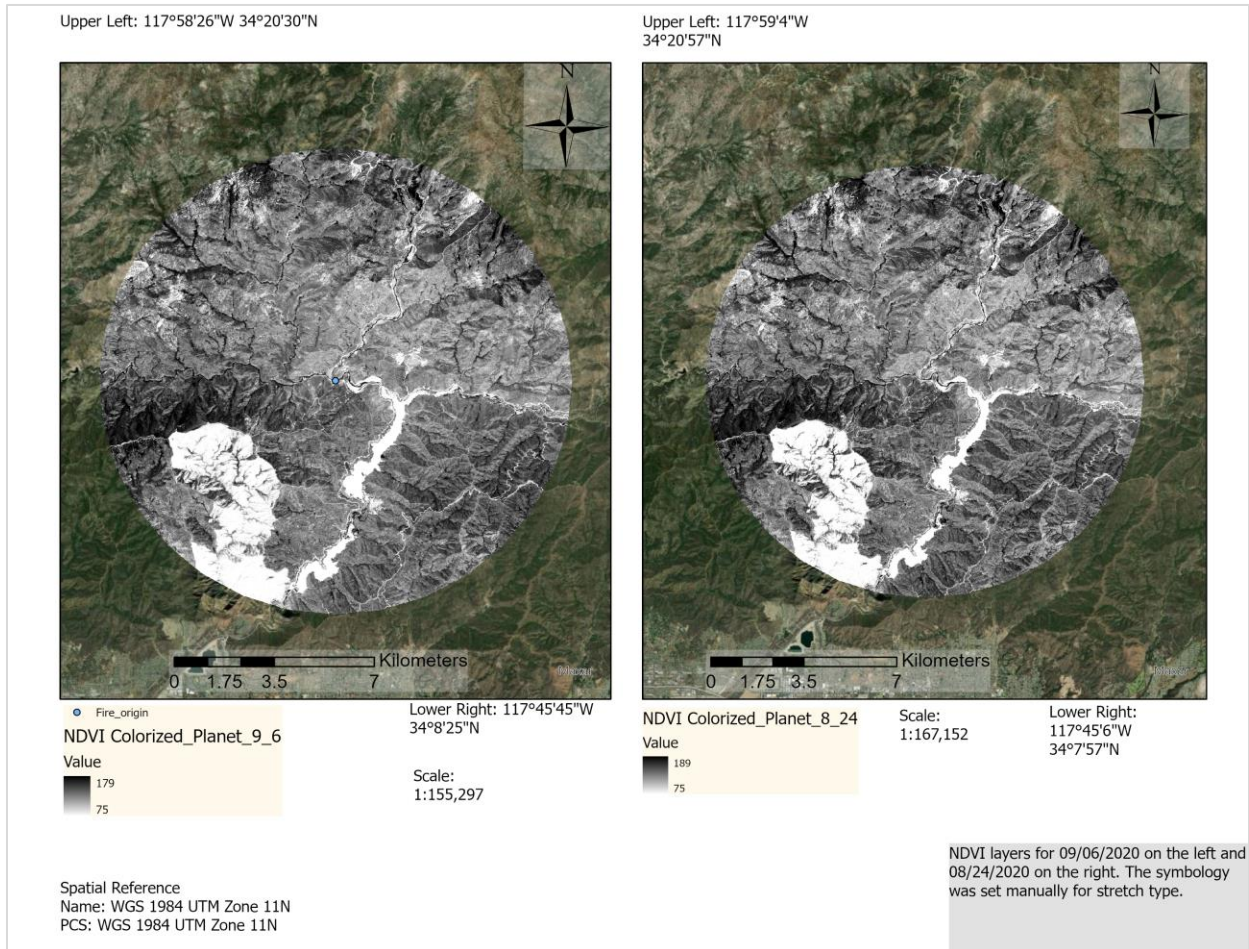


Figure 20. NDVI maps for 09/06/2020 (left) and 08/24/2020 (right), PlanetScope Scenes.

conditions that existed prior to the fire outbreak. As vegetation was drying it was slowly creating a combustible fuel for a potential fire event.

#### *4.3.4. Rescale by Function*

Because the values of each dataset are relative to the criteria they represent before integrating them and weight these criteria relative to each other a susceptibility assessment had to transform their values to a common scale. Reclass by Function tool transforms all four raster layers. For Hillshade, Slope, and NDVI layers project applied reclass by scale large function. A large function preferentially favors large values, where the midpoint parameter defines the transition point of function. DA layer used linear rescaling. Contrary to the large function, the linear function in the fire susceptibility model favored values that increased at the constant rate from the road. Functions behavior and graphs are discussed in more details in publication by Jiang and colleagues (Jian et al. 2000).

#### *4.3.5. Weighted Susceptibility Results (Soft Classification)*

Each previously described layer was weighted with the Weighted Sum tool. In Figure 21 (1-2) maps were displaying areas that were more susceptible based on the input parameters. The weighted values were set to 1 for NDVI and Slope layers while for the DA layer the value was set to -1. The negative value for the DA layer was selected for the purpose of inverting the results from the rescale by function operation. This flipped the results while at the same time preferentially weighted areas closer to a road as more susceptible on the scale from -10 to -1, where -1 was more susceptible. For the Hillshade layer the value was set to 0.3. The weighting was done arbitrarily where the coefficient values did not represent the best possible parametrization but rather it laid down a methodology for a potential end user of this method.

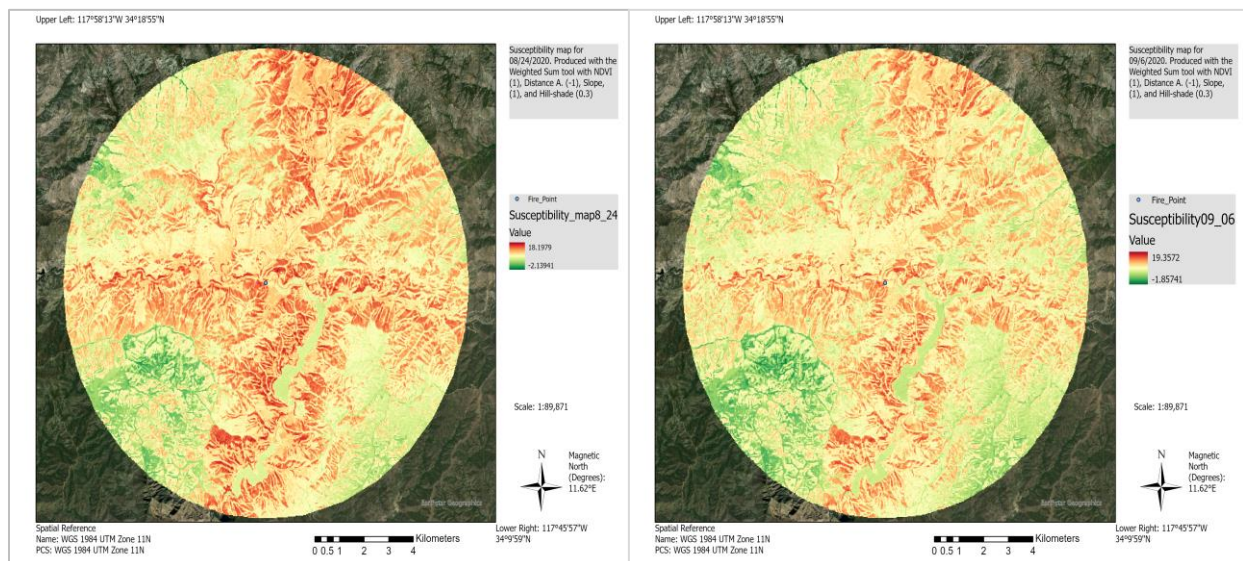


Figure 21 (1-2). Susceptibility maps 8/24/20 (left) and 09/06/20 (right).

Maps are showing the extent of PlanetScope image capture. The capture area represented the smallest spatial resolution for this project centered around fire outbreak origin which was marked with a blue dot.

A green surface area that cut through the southern centered region lay on top of San Gabriel reservoir. Water's flat surface area had a 0 Slope thus once the Slope layer was weighted with Weighted Sum tool then the reservoir area was deemed not-susceptible. Both dates on above maps, when compared, showed similar spatial distribution of susceptible areas.

Map products from a Figure 21 (1-2) were geo-processed with Reclassify raster tool where classification method created two classes, susceptible 1 and non-susceptible 0. Reclassify raster threshold was set to 0 from -2.139 to 17 and as unsusceptible and to 1 from 17-18.19 as susceptible for 8/24/2020, and to 0 from -1.875 to 17 as unsusceptible and 1 from 17-19.357 as susceptible. Classification threshold values were chosen after the original layers from the figure

were manually classified in the Symbology tab (Figure 22. 1-2). Again, this study was aware that this was not the best possible fit but one of many solutions.

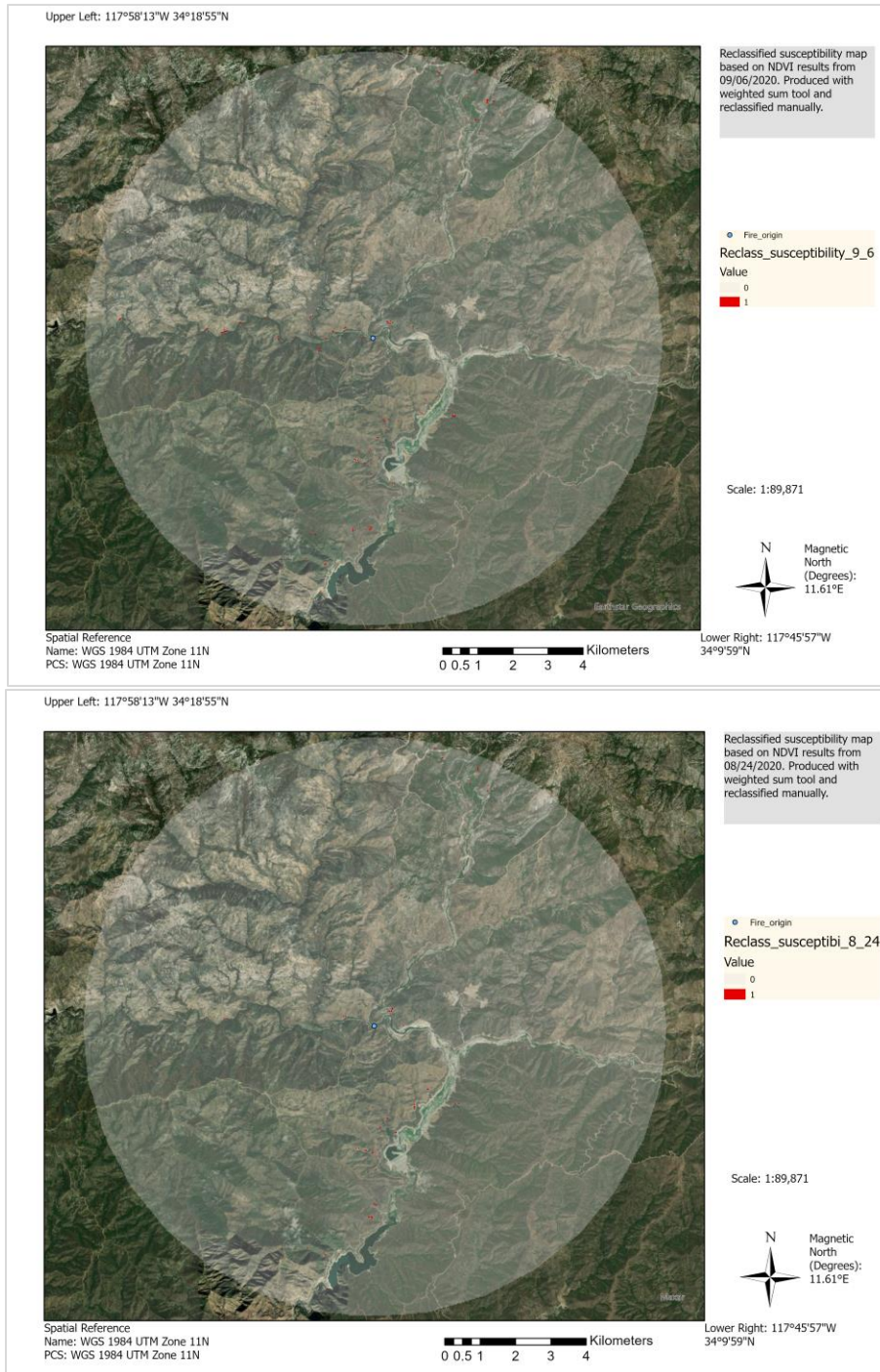


Figure 22 (1-2). Reclassed Susceptibility maps 8/24/20 (bottom) and 09/06/20 (top).

#### *4.3.6. Manual -Hard Classification Susceptibility Results*

Similarly, to Weighted semi-soft classification approach manual hard-classification methodology delivered two susceptibility maps for two dates. Two-week time difference was picked arbitrarily for comparison. Based on the original goal where first responders and local authorities had to respond to rapidly deteriorating ground conditions by running frequent GIS assessments. Based on the original goal where first responders and local authorities had to respond to rapidly deteriorating ground conditions by running frequent GIS assessments. Since the Santa Ana winds were present, low humidity had already persisted before the fire erupted. The idea behind these approaches was to have multiple models and methodologies ready for daily assessment.

Two products delineated fire prone zones in red, labeled 1 on the Legend section (Figure 23.1-2). The rest of AOI was labeled 0 and manually changed into transparent gray. Interestingly, both map products labeled fire origin location as susceptible. Contrary to the weighted model that produced less susceptible regions by surface area and more dispersed pattern. This modeling approach appeared more accurate.

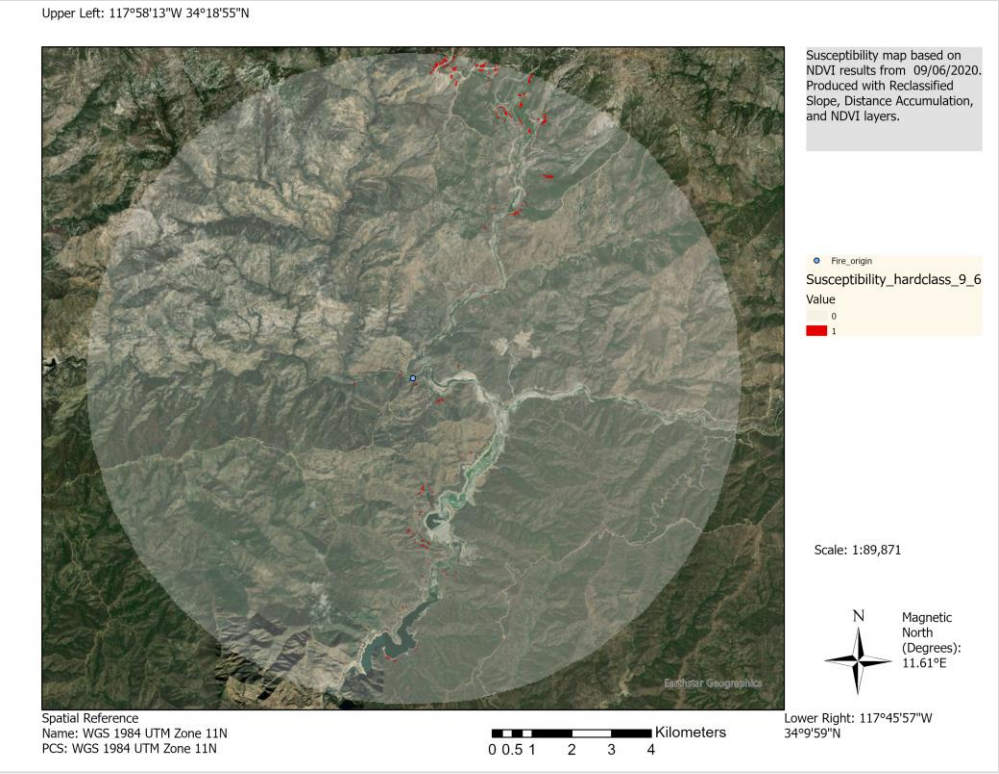
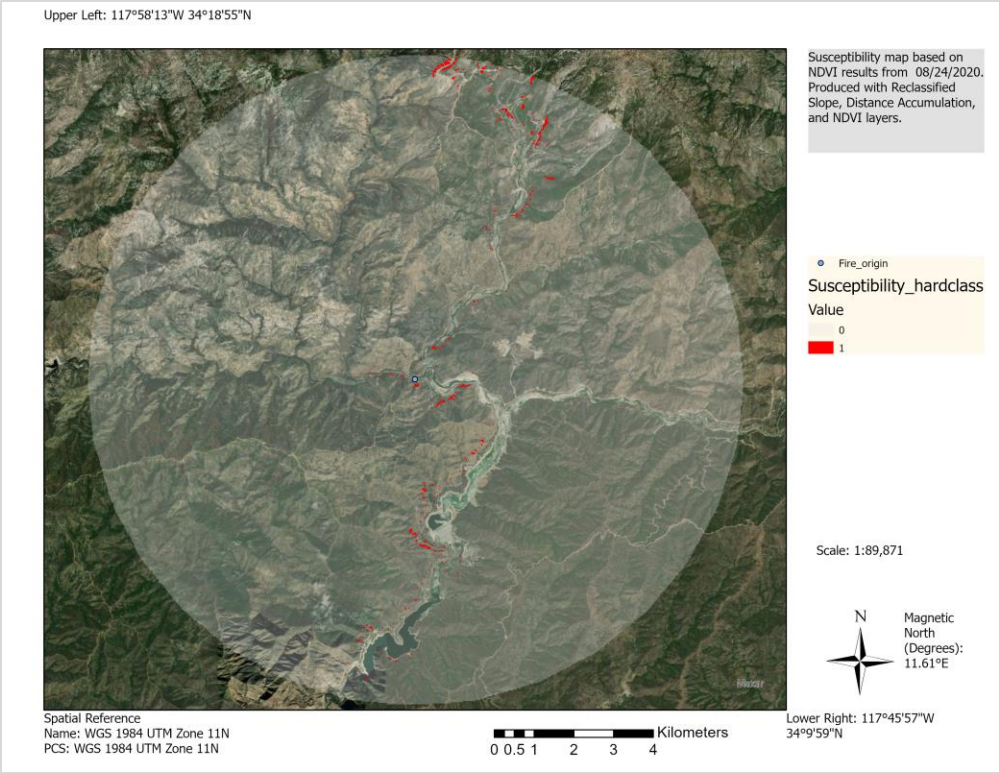


Figure 23 (1-2). Manual hard-reclassified susceptibility maps; 08/24/2020 (top) and 09/06/2020 (bottom)

### 4.3.7. Electric Lines

To avoid similar outbreaks susceptibility assessment produced a reclassified transmission lines susceptibility map. In Figure 24 green lines represented areas where transmission lines were passing through vegetation. Chapter 3 described that vegetation presence was detected using NDVI indices derived from PlanetScope imagery. Purple areas were classified as less susceptible. However, the cutoff between both classes should be examined by the end user of this product on the ground.

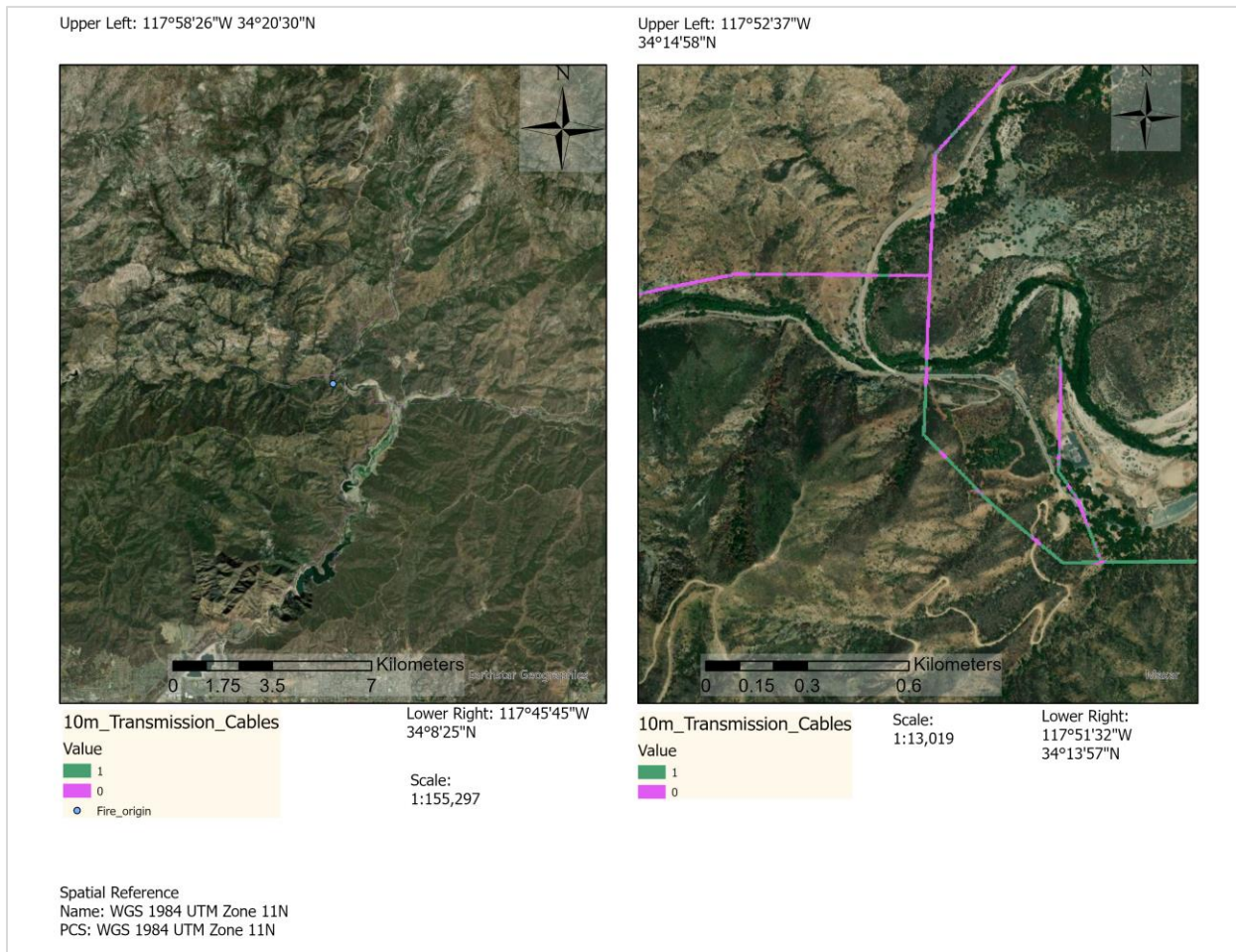


Figure 24. Electric lines (Buffered 3m, converted to raster, and combined with NDVI layer with Raster Calculator tool)

## **4.4. Synthesizing and Comparing Different Extents and Resolutions**

The following results compared the coarse resolution results, Southern California extent with Los Angeles County and finally Los Angeles County extent with a section of Angeles National Forest. This comparison was done between maps produced with MODIS, DEM, and Planet resolutions.

### *4.4.1. Overlaying Susceptibility and Electric Lines Maps*

On the fine scale, this subsection integrated reclassified weighted and hard classification map products with electric lines susceptibility map. To illustrate the relationship between Slope, Aspect, DA, Electric lines, and NDVI two maps for two different dates, 08/24/2020 and 09/06/2020, are shown in Figure 25. Despite the positive results, the application of overlaying different layers is limited to local topographic and climate features.

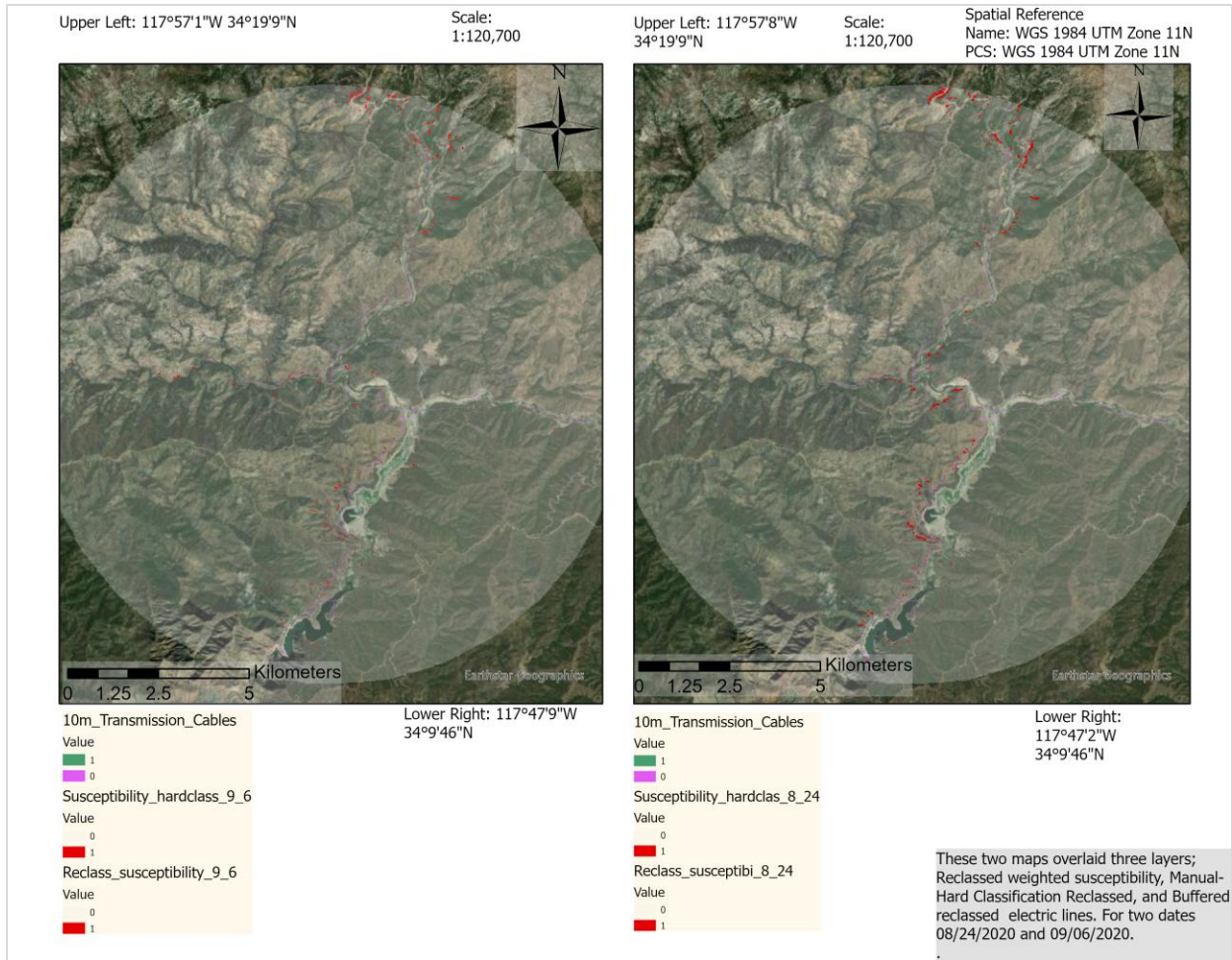


Figure 25 Synthesized susceptibility maps for 08/24/2020 (right) and 09/06/2020 (left)

#### 4.4.2. Comparing Two Scenarios-MODIS Resolution

When NMDI and NDWI results were compared with raster trend, prediction, and argument statistics results this project observed that the aforementioned drought indices spatial distribution was showing similar fitness for use as raster predictive models.

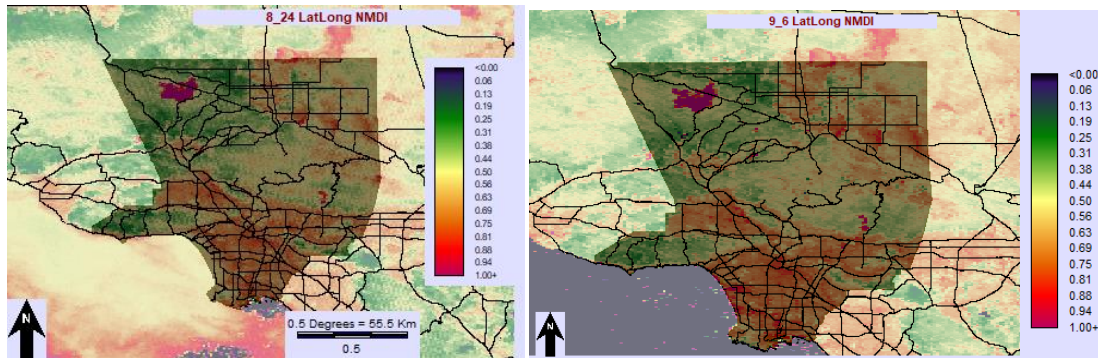


Figure 26. Spatial distribution of NMDI over Los Angeles County 08/24/2020, left, and 09/06/2020, right, overlaid with road network shapefile.

Figures 12 (1-3), 13 (1-3), 14, 15, and 16 the areas that were outside the Angeles national forest were showing a higher rate for pixel change. This was most likely due to the lack of vegetation in that area. The bare soil accumulates more radiation thus the surface reflectance in the IR spectrum was substantially higher when compared to vegetation covered areas.

Similarly, Figure 26 shows that vegetation covered areas returned pixel values that were less than non-vegetation covered. The remote sensing of both soil and vegetation water content from space by using three channels centered near 860 nm, 1640 nm and 2130 nm has shown results that were consistent with expectations, Figures 17, Appendix: NMDI and NDWI, and 25.

#### *4.4.3. MODIS and DEM-PlanetScope Comparison*

As conditions on the ground were rapidly changing during August 2020, then susceptible areas would have needed to be delineated as wildfires were raging across California.

In the hypothetical scenario first responders could perform parallel analyses with coarse, medium, and fine scale resolutions. Ideally first responders would detect an anomaly centered around a road network from space platforms, such as MODIS, with coarse resolution. Then run a finer scale analysis, PlanetScope, to refine and pinpoint high-risk areas. The preliminary results, suggested that this scenario where a pixel will be mapped as dry soil condition if the NMDI is  $>0.7$ , intermediate if NMDI is within the range of 0.6 to 0.7, and wet if NMDI is  $<0.6$  did not delineate sufficiently small area. Similarly, to NMDI NDWI has shown similar performance.

The area that could be further scaled down, where adding ancillary datasets such as Slope and Hillshade could pinpoint hazard areas with higher confidence. Even though the DEM-PlanetScope model mapped susceptible areas that included fire outbreak location this was done with hindsight bias. This project opted to perform reverse engineering and look for linkage between different scenario-based models. However, this work did not find solid linkage between previously mentioned scenarios.

## Chapter 5 Discussion

This project's objective was to compare remote sensing platforms' utility for pre-fire assessment. MODIS, DEM, and Planet data were manipulated with three different scenarios to estimate the spatial and temporal distribution of fire indices and topographic variables. This project's collateral goal was to provide valuable insight to first responders and land management agencies. This chapter emphasizes the inferences from this thesis, together with the obstacles and limitations. In addition, the future research was also brought up with a more in-detail assessment of methods and workflows in order to expand and better this work.

### 5.1. Discussion

Monitoring the severity and attributes of drought was crucial in modern pre-fire assessment and risk management. Despite the wide range of studies and funding it was still an elaborate assessment. In general wildfire susceptibility scenario-based assessment had two approaches one was dynamic analysis where a research focused on meteorological variables and the second is topographic analysis where the research evaluated how the terrain structure affected fire outbreaks.

However, these scenario-based models were not scale immune. That issue does raise a question on how these models perform when the area of interest shifts to a different region. By just moving to Northern California this project would encounter different vegetation types and agricultural practices.

In the previous chapters, namely 3 and 4, the analysis was performed with three different spatial and radiometric resolutions. The results were mixed and the MODIS' instrument spatial-temporal analysis did not yield sufficiently small delineation of fire hazardous areas. The NDWI and NMDI analysis did suggest that the region as a whole was becoming highly flammable while

the area in immediate proximity of the fire outbreak did not return pixel values that could be classified as hazardous. The expectations were that coarse scale analysis would point out sufficiently small regions that could be further in-depth analyzed with ancillary datasets such as road and electric networks.

Wildfires were not exclusive to the California region and many publications have described different approaches to model and map wildfire susceptibility. Some work approached from different perspectives and used the nearest-neighbor method. This was done by Amatulli and colleagues (Amatulli, Perez-Cabello, and Riva 2007) where the assessment used interpolation tools to map wildfires caused by human and thunder strikes.

## **5.2. Limitations**

The triple scenario presented in this work has brought some insightful findings. Results presented insofar account for a small part of what is necessary to create a more in-depth susceptibility assessment. While NMDI and NDWI indices were crucial to understand what areas were the most impacted by drought, the presence of man-made infrastructure dictated the hazard of fire outbreak.

### *5.2.1. NMDI and NDWI*

Producing both indices with IDRISI TerrSet was straightforward and relatively easy to complete. One advantage that this project had was the availability of preprocessed MODIS data. Previous chapters pointed out that MODIS MOD09GA Version 6.1 data was corrected for atmospheric gasses. This thesis used corrected images for NMDI and NDWI indices estimation. This was done to accelerate the workflow and bypass conversion of DN values into spectral radiance. First responders or responsible agencies would have extra steps and correct acquired

images. The end user would acquire almost in-real-time imagery and then perform atmospheric correction.

### *5.2.2. Multidimensional Analysis*

Raster predictive analysis produced some interesting results compared to NMDI and NDWI analysis. However, this was the most time-consuming part of the study. Building multidimensional datasets where 7 mosaiced datasets were created took approximately two hours. Additional time, two days in total, was spent on rendering data and producing Temporal Chart profiles, Trend Analysis, Prediction Tool, and Argument Statistic CRF file. Raster predictive analysis had some stumbling blocks throughout the tool's execution. Trend Analysis produced results only with second degree polynomial function. At first it was unclear why harmonic function choice did not work but after reviewing function's utility it was clear that 2nd degree polynomial function fitted data that had more fluctuations.

Predict tool produced results based on trend analysis. Therefore, the slope trend of pixel change in trend analysis was determining the future trends. Hence, results amplified the existing slope trend. Pixels that had a bigger slope change were projected to have higher values. This feature could lead to a somehow incorrect map interpretation since this method did not consider weather oscillations. Oscillatory nature of weather in Southern California was controlled by penetrations of ocean air masses and desert dry air masses. Thus, any predictive analysis on the Los Angeles County scale could lead to ambiguous results.

### *5.2.3. Susceptibility Analysis and Ground Truthing*

A more responsible land and forest management system would benefit if pre-fire susceptibility mapping methodology was predetermined by authorities. When estimating human dwelling range with Distance Accumulation equation (4) and overlaying it with DEM layer and

its derivatives (Slope and Hillshade), Planet Scope NDVI, and adding Transmission lines then the results from analysis came spatially close to the fire outbreak origin. Some map products actually overlapped the susceptibility areas with the fire origin. Perhaps, armed with hindsight this project was unintentionally nudging parameters so the result came close to outbreak point.

However, the aforementioned mapping approach was validated by coming spatially close to the point of fire origin. What this project wanted was to use methods that were already there and modify them thus when the pre-fire conditions are present then the local authorities can have a workflow for mapping in place.

### **5.3. Future Research**

The findings presented in this work represented a fraction of possible pathways that could produce fire susceptible areas. The additional steps in this research would be to include Notebook Python environments, VIIRS satellite data, and county scale electric road networks analysis.

#### *5.3.1. Model-builder vs. Notebook Environment*

The simplified Model-builder often failed while Notebook performance was much faster and storage efficient, table 6. This was a great advantage over Model-builder that creates an output file. An output file occupied storage space, 117,19MB. Frequently, throughout this thesis minor glitches and wrong parametrization would produce both an erroneous layer and empty layer. From this thesis work experience future projects could perform more efficiently if they rely more on the Notebook environment. Moreover, a combination of both compliments each other. This was evident when inputting a DA layer into the geoprocessing interface. Because an interface allows data reading, then from the readings it was possible to adjust settings in the Notebook code line.

Tool	Model-Builder	Notebook environment (Python)
Execution Time (Rescale by Function)	Application Stopped working or ArcGIS Pro issue coded warning	41 seconds

Table 6. Model-builder versus Notebook.

### 5.3.2. Adding VIIRS product

The Suomi National Polar-orbiting Partnership (SNPP) platform-based NASA VIIRS L1B calibrated radiances product derived from the five image-resolution or I-bands, which have a 375-meter resolution at nadir. These I-bands comprise three reflective solar bands (RSB) and two thermal emissive bands (TEB). Each of the I-bands has 32 detectors in the along-track direction with 32 rows of pixels per scan. Ranging in wavelengths from 0.6  $\mu\text{m}$  to 12.4  $\mu\text{m}$ , the I-bands are sensitive to visible/reflective, near-, shortwave-, mediumwave-, and longwave-infrared wavelengths. In contrast to a MODIS L1B product, which temporally spans 5 minutes, the VIIRS L1B calibrated radiances product contains a nominal temporal duration of 6 minutes.

This spatial and radiometric resolution would be used to calculate an additional raster predictive model. Also, 375-meter resolution would be used for coarse scale susceptibility analysis. Therefore, a comparison between two different resolutions would test both susceptibility approaches with more rigor.

## 5.4. Conclusion

This thesis partially achieved its results when assessing scenarios for pre-fire susceptibility, raster predictive, and drought indices models. These pre-fire susceptibility map products were compared to raster predictive maps and regional indices maps. A comparison found that there was very little or no relationship between raster predictive, regional, and

susceptibility analysis. In the future, the methodology would include overlapping electric and road networks with coarse scale pre-fire indices analysis. In addition, data-processing would include more Notebook Python environment data processing, thus speeding up some steps that this thesis found time consuming.

Wildfires pose a substantial risk that must be mitigated by local first responders and land management agencies. This thesis might provide some intuition to previously mentioned organizations.

## References

- Adab, Hamed, Kasturi Devi Kanniah, and Jason Beringer. 2016. "Estimating and up-Scaling Fuel Moisture and Leaf Dry Matter Content of a Temperate Humid Forest Using Multi Resolution Remote Sensing Data." *Remote sensing (Basel, Switzerland)* 8, no. 11: 961–961.
- Afonso, Ricardo, André Neves, Carlos Viegas Damásio, João Moura Pires, Fernando Birra, and Maribel Yasmina Santos. 2020. "Assessment of interventions in fuel management zones using remote sensing." *ISPRS International Journal of Geo-Information* 9, no. 9: 533.
- AghaKouchak, Amir, A. Farahmand, F. S. Melton, J. Teixeira, M. C. Anderson, Brian D., 2015. Wardlow, and C. R. Hain. "Remote sensing of drought: Progress, challenges and opportunities." *Reviews of Geophysics* 53, no. 2: 452-480.
- Álvarez, Christian Adrián, and Noel Carbajal. 2019. "Regions of Influence and Environmental Effects of Santa Ana Wind Event." *Air quality, atmosphere and health* 12, no. 9: 1019–1034.
- Amatulli, Giuseppe, Fernando Pérez-Cabello, and Juan de la Riva. 2007. "Mapping lightning/human-caused wildfires occurrence under ignition point location uncertainty." *Ecological modelling* 200, no. 3-4: 321-333.
- Bachmann, A. and Allgoewer, B. 1999. The need for a consistent wild- fire risk terminology, in: *Proceedings of the Joint Fire Science Conference and Workshop, Boise Idaho, 15–17 June 1999.*
- Barmpoutis, Panagiotis, Periklis Papaioannou, Kosmas Dimitropoulos, and Nikos Grammalidis. 2020. "A review on early forest fire detection systems using optical remote sensing." *Sensors* 20, no. 22: 6442.
- Boyd, D. S, and F. M Danson. 2005. "Satellite Remote Sensing of Forest Resources: Three Decades of Research Development." *Progress in physical geography* 29, no. 1: 1–26.
- Beighley, M. 2009. Forest defense against fire in Portugal, situation and capability, *The Forest, the Path to sustainable prosperity – International Seminar, Lisbon, 2 June 2009.*
- Campbell, James B., and Randolph H. Wynne. 2011. *Introduction to remote sensing.* Guilford Press.
- Ceccato, Pietro, Stephane Flasse, and Jean-Marie Gregoire. 2002. "Designing a spectral index to estimate vegetation water content from remote sensing data: Part 2. Validation and applications." *Remote Sensing of Environment* 82, no. 2-3: 198-207.
- Chowdhury, Ehsan H, and Quazi K Hassan. 2015. "Development of a New Daily-Scale Forest Fire Danger Forecasting System Using Remote Sensing Data." *Remote sensing (Basel, Switzerland)* 7, no. 3: 2431–2448.

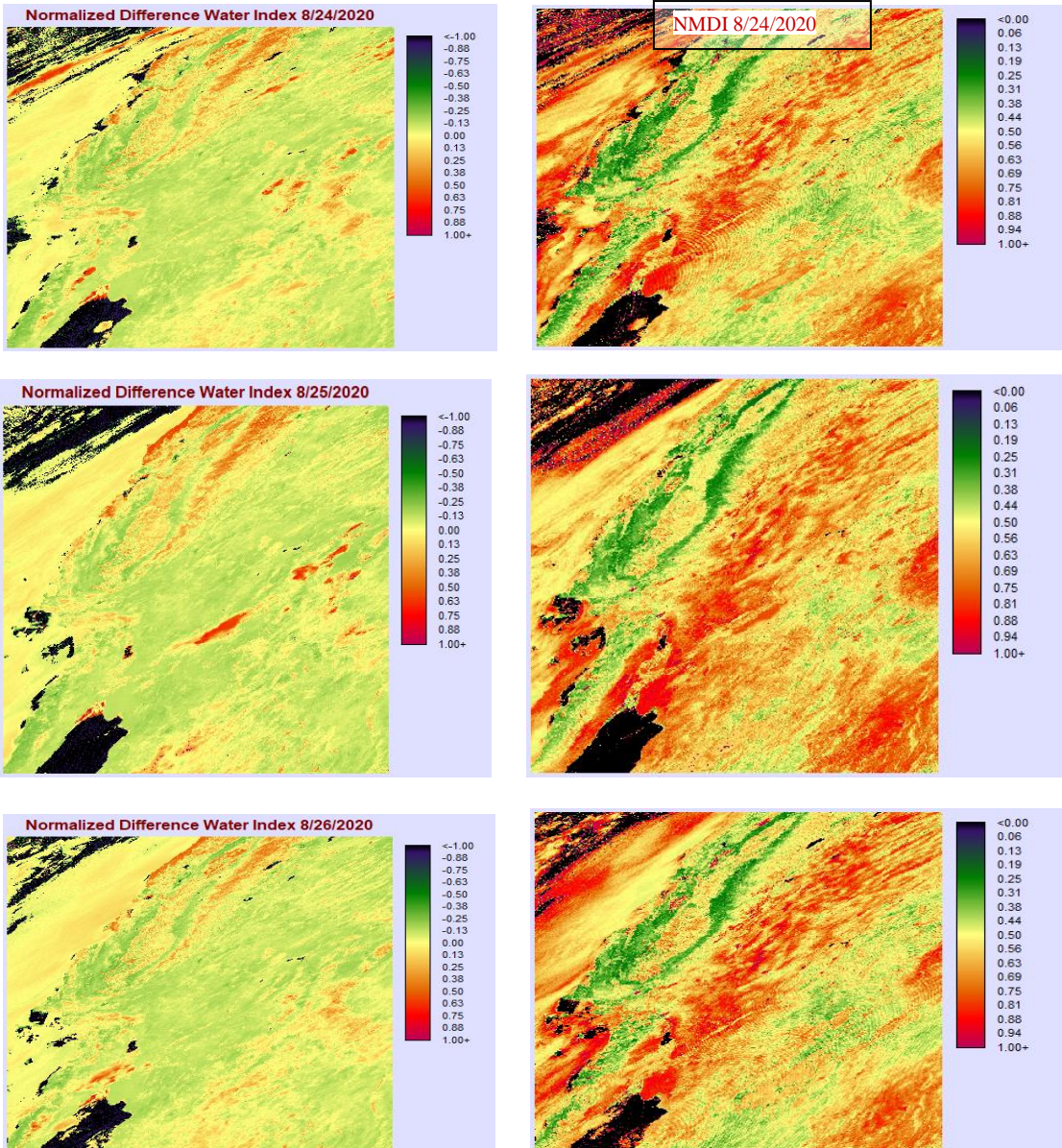
- Chuvieco, Emilio, Inmaculada Aguado, Javier Salas, Mariano García, Marta Yebra, and Patricia Oliva. 2020. "Satellite Remote Sensing Contributions to Wildland Fire Science and Management." *Current Forestry Reports* 6, no. 2: 81–96.
- Csillik, Ovidiu, Pramukta Kumar, and Gregory P Asner. 2020. "Challenges in Estimating Tropical Forest Canopy Height from Planet Dove Imagery." *Remote sensing (Basel, Switzerland)* 12, no. 7: 1160–.
- Csiszar, Ivan, Wilfrid Schroeder, Louis Giglio, Evan Ellicott, Krishna P Vadrevu, Christopher O Justice, and Brad Wind. 2014. "Active Fires from the Suomi NPP Visible Infrared Imaging Radiometer Suite: Product Status and First Evaluation Results." *Journal of geophysical research. Atmospheres* 119, no. 2: 803–816.
- Delbart, Nicolas, Laurent Kergoat, Thuy Le Toan, Julien Lhermitte, and Ghislain Picard. 2015. "Determination of phenological dates in boreal regions using normalized difference water index." *Remote Sensing of Environment* 97, no. 1: 26-38.
- Delfino, Ralph J., Sean Brummel, Jun Wu, Hal Stern, Bart Ostro, Michael Lipsett, Arthur Winer et al. 2009. "The relationship of respiratory and cardiovascular hospital admissions to the southern California wildfires of 2003." *Occupational and environmental medicine* 66, no. 3: 189-197.
- Gao, Bo-Cai. 1996. "NDWI—A normalized difference water index for remote sensing of vegetation liquid water from space." *Remote sensing of environment* 58, no. 3: 257-266.
- Goodchild, M F. 1977. "An Evaluation of Lattice Solutions to the Problem of Corridor Location." *Environment and planning. A*9, no. 7: 727–738.
- Gould, Peter R. 1967. "On the geographical interpretation of eigenvalues." *Transactions of the Institute of British Geographers*: 53-86.
- Giglio L, Schroeder W, Justice CO. 2016. The collection 6 MODIS active fire detection algorithms and fire products. *Remote sensing of the environment*. 2016; 178: 31-41.doi: 10.1016/j.rse.02.054
- Gu, Yingxin, Eric Hunt, Brian Wardlow, Jeffrey B. Basara, Jesslyn F. Brown, and James P. Verdin. 2008. "Evaluation of MODIS NDVI and NDWI for vegetation drought monitoring using Oklahoma Mesonet soil moisture data." *Geophysical Research Letters* 35, no. 22.
- Han, K., Viau, A. A., & Anctil, F. 2003. High-resolution forest fire weather index computations using satellite remote sensing. *Canadian Journal of Forest Research*, 33(6), 1134-1143.
- Hendel, Isabelle-Gabriele, and Gregory M. Ross. 2020. "Efficacy of remote sensing in early forest fire detection: A thermal sensor comparison." *Canadian Journal of Remote Sensing* 46, no. 4: 414-428.

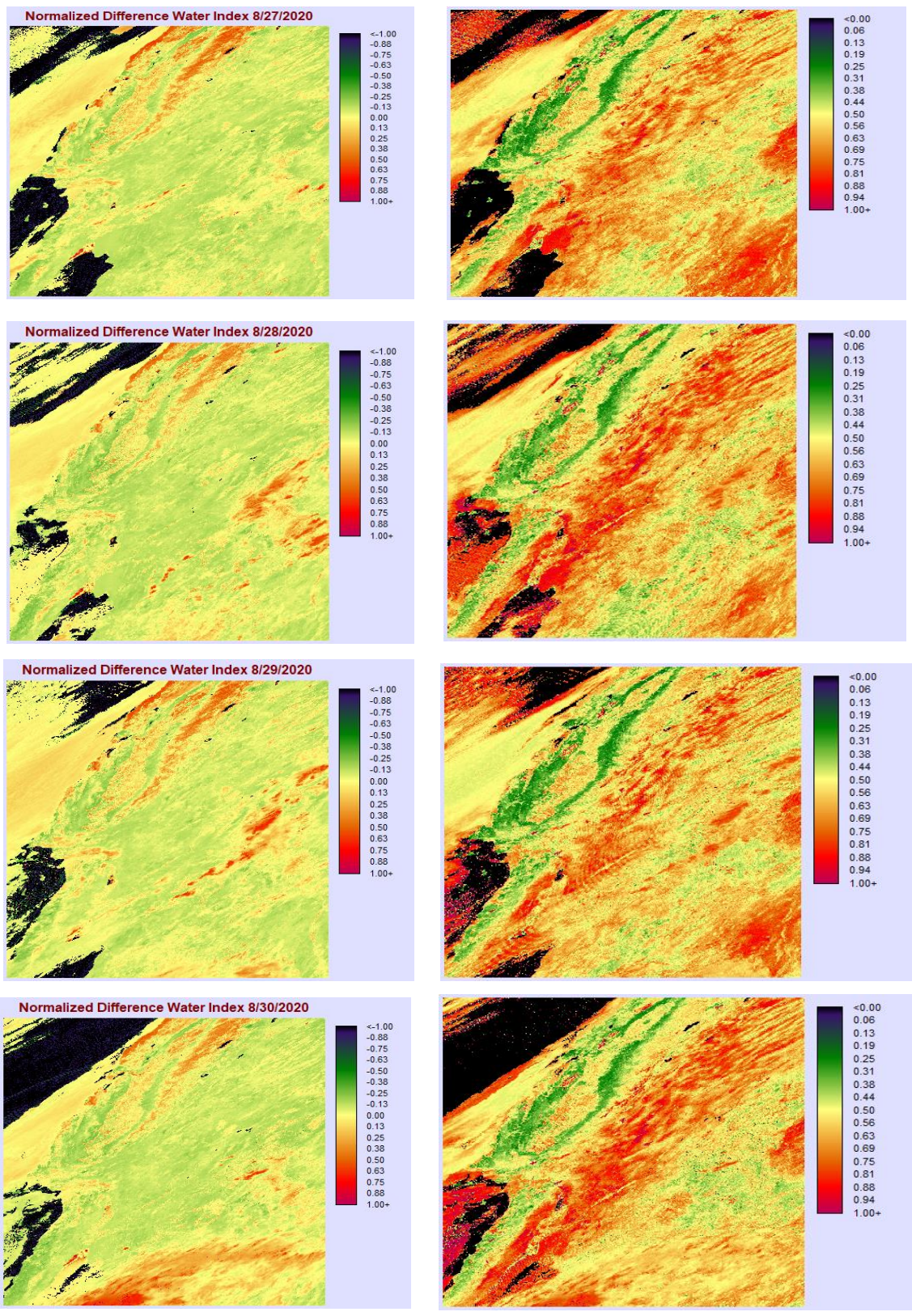
- Henderson, Sarah B., Michael Brauer, Ying C. MacNab, and Susan M. Kennedy. 2011. "Three measures of forest fire smoke exposure and their associations with respiratory and cardiovascular health outcomes in a population-based cohort." *Environmental health perspectives* 119, no. 9: 1266-1271.
- Hauptman, Marissa, John R Balmes, and Mark D Miller. 2020. "The Hazards of Wildfire Smoke Exposure for Children." *Current problems in pediatric and adolescent health care* 50, no. 2: 100756–100756.
- Hu, Fei, Chaowei Yang, Yongyao Jiang, Yun Li, Weiwei Song, Daniel Q Duffy, John L Schnase, and Tsengdar Lee. 2020. "A Hierarchical Indexing Strategy for Optimizing Apache Spark with HDFS to Efficiently Query Big Geospatial Raster Data." *International journal of digital earth* 13, no. 3: 410–428.
- Ingersoll, Raymond V, and Peter E Rumelhart. 1999. "Three-Stage Evolution of the Los Angeles Basin, Southern California." *Geology (Boulder)* 27, no. 7: 593–596.
- Littell, Jeremy S, David L Peterson, Karin L Riley, Yongquiang Liu, and Charles H Luce. 2016. "A Review of the Relationships Between Drought and Forest Fire in the United States." *Global change biology* 22, no. 7: 2353–2369.
- Jia C. Liu, Gavin Pereira, Sarah A. Uhl, Mercedes A. Bravo, Michelle L. Bell. 2015. A systematic review of the physical health impacts from non-occupational exposure to wildfire smoke, *Environmental Research*, Volume 136, Pages 120-132, ISSN 0013-9351.
- Jiang, Hong, and J. Ronald Eastman. 2000. "Application of fuzzy measures in multi-criteria evaluation in GIS." *International Journal of Geographical Information Science* 14, no. 2: 173-184.
- "Los Angeles: Geography and Climate." *Cities of the United States*, 2006. Detroit, MI: Gale. *Gale eBooks* (accessed October 22, 2021).
- Madden, Austin. 2020. "Use Multidimensional Data and Tools in ArcGIS Pro." Earthdata, last modified on October 02, 2020, <https://wiki.earthdata.nasa.gov/display/SDT/Use+Multidimensional+Data+and+Tools+in+ArcGIS+Pro>.
- Marder, Jenny. 2019. "NASA Tracks Wildfires from Above to Aid Firefighters Below." NASA Goddard Space Flight Center, last updated July 31, 2019, <https://www.nasa.gov/feature/goddard/2019/nasa-tracks-wildfires-from-above-to-aid-firefighters-below>.
- Morisette, Jeffrey T, Louis Giglio, Ivan Csiszar, Alberto Setzer, Wilfrid Schroeder, Douglas Morton, and Christopher O Justice. 2005. "Validation of MODIS Active Fire Detection Products Derived from Two Algorithms." *Earth interactions* 9, no. 9: 125.

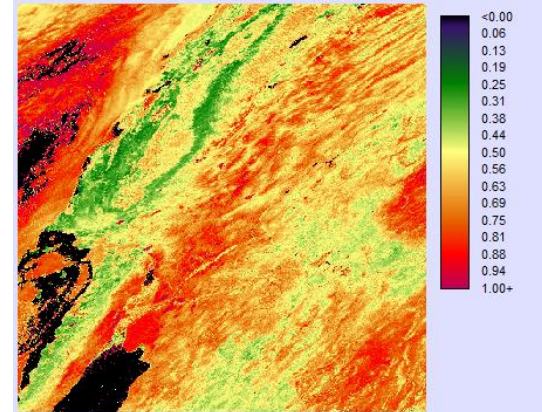
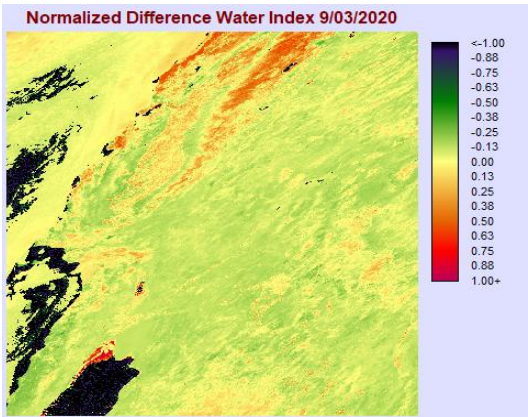
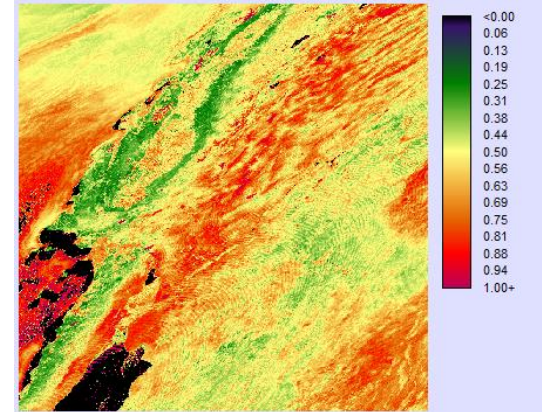
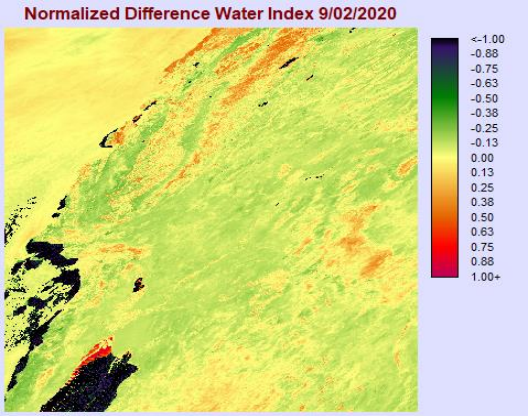
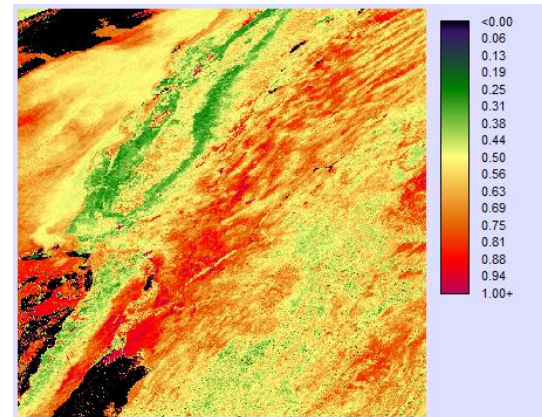
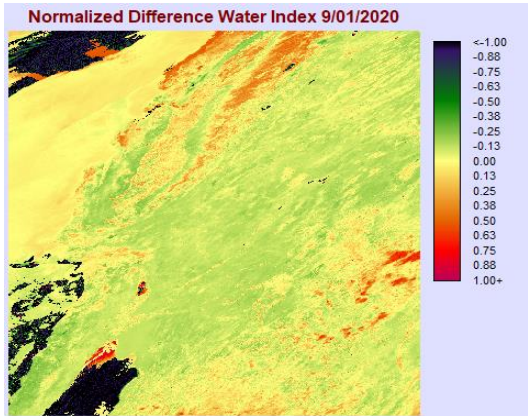
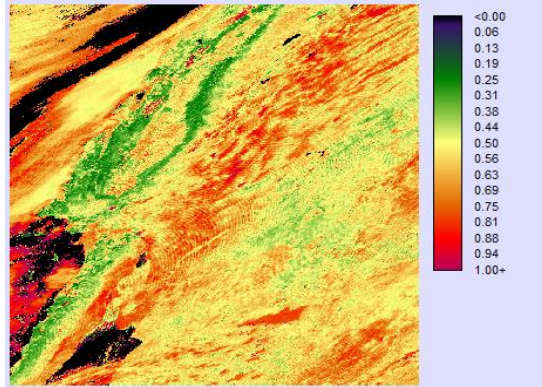
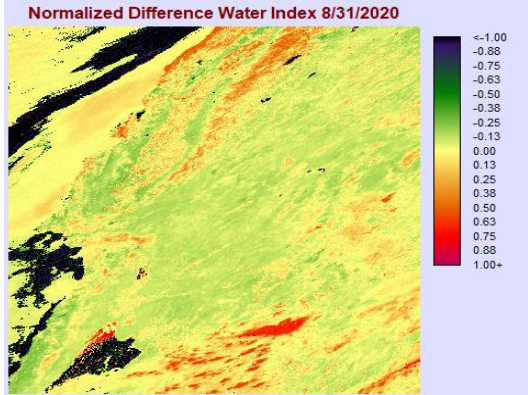
- Naeher, Luke P., Michael Brauer, Michael Lipsett, Judith T. Zelikoff, Christopher D. Simpson, Jane Q. Koenig, and Kirk R. Smith. 2007. "Woodsmoke health effects: a review." *Inhalation toxicology* 19, no. 1: 67-106.
- Phuleria HC, Fine PM, Zhu Y. 2005. Air quality impacts of the October 2003 Southern California wildfires. *J Geophys Res*:110. <https://doi.org/10.1029/2004JD004626>
- Reid CE, Jerrett M, Tager IB, Petersen ML, Mann JK, Balmes JR. 2016. Differential respiratory health effects from the 2008 northern California wildfires: a spatiotemporal approach. *Environ Res*; 150:227–35.
- Rokni, K., Ahmad, A., Solaimani, K., and Hazini, S., 2016. A new approach for detection of surface water changes based on principal component analysis of multitemporal normalized difference water index. *Journal of Coastal Research*, 32(2), 443–451. Coconut Creek (Florida), ISSN 0749-0208.
- Salajanu, D, and C.E Olson. 2001. "The Significance of Spatial Resolution: Identifying Forest Cover from Satellite Data." *Journal of forestry* 99, no. 6: 32–38.
- Salguero, John, Jingjing Li, Alireza Farahmand, and John T Reager. 2020. "Wildfire Trend Analysis over the Contiguous United States Using Remote Sensing Observations." *Remote sensing (Basel, Switzerland)* 12, no. 16: 2565–.
- Salis, Michele, Alan A Ager, Fermin J Alcasena, Bachisio Arca, Mark A Finney, Grazia Pellizzaro, and Donatella Spano. 2015. "Analyzing Seasonal Patterns of Wildfire Exposure Factors in Sardinia, Italy." *Environmental monitoring and assessment* 187, no. 1: 1–20.
- Schroeder, W., Oliva, P., Giglio, L., & Csizsar, I. A. 2014. The New VIIRS 375m active fire detection data product: algorithm description and initial assessment. *Remote Sensing of Environment*, 143, 85-96.
- Shimizu, Katsuto, Tetsuji Ota, Nobuya Mizoue, and Hideki Saito. 2020. "Comparison of Multi-Temporal Planetscope Data with Landsat 8 and Sentinel-2 Data for Estimating Airborne LiDAR Derived Canopy Height in Temperate Forests." *Remote sensing (Basel, Switzerland)* 12, no. 11: 1876–.
- USDA Forest Service. "The Rising Cost of Fire Operations: Effects on the Forest Service's Non-Fire Work." . 2014.
- Vadrevu, Krishna, and Kristofer Lasko. 2018. "Intercomparison of MODIS AQUA and VIIRS I-Band Fires and Emissions in an Agricultural Landscape-Implications for Air Pollution Research." *Remote sensing (Basel, Switzerland)* 10, no. 7: 978–978.
- Verde, J.C, and José Luis Zêzere. 2010. "Assessment and Validation of Wildfire Susceptibility and Hazard in Portugal." *Natural hazards and earth system sciences* 10, no. 3: 485–497.

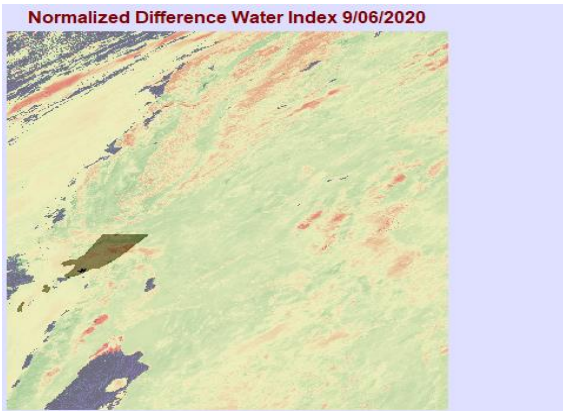
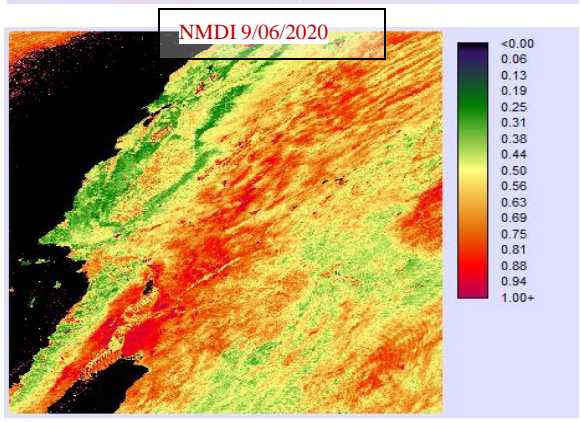
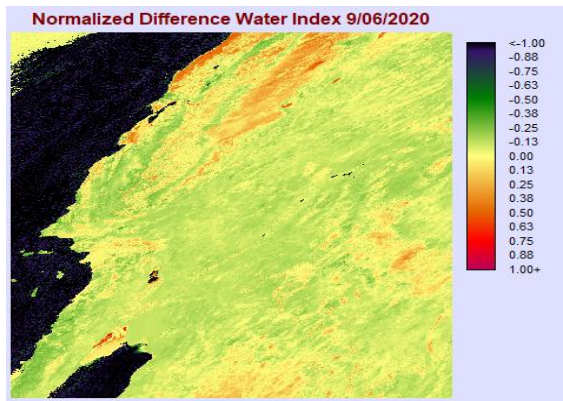
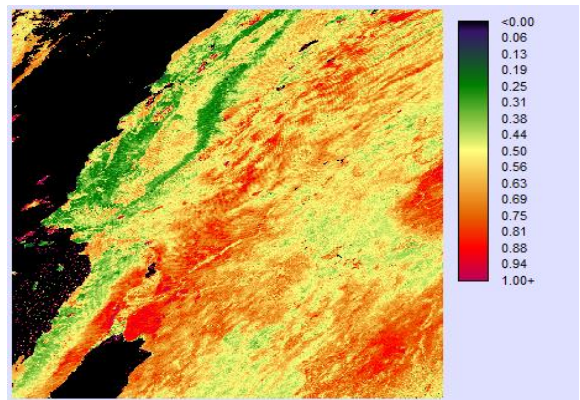
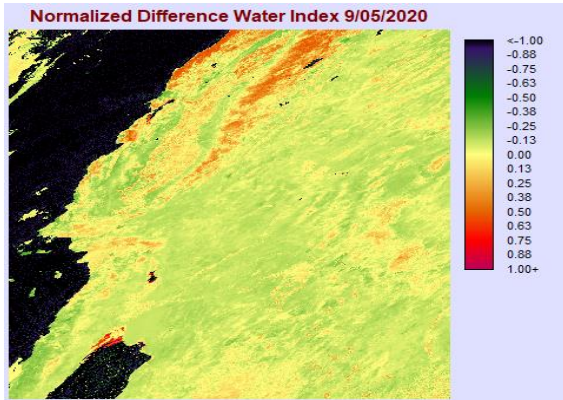
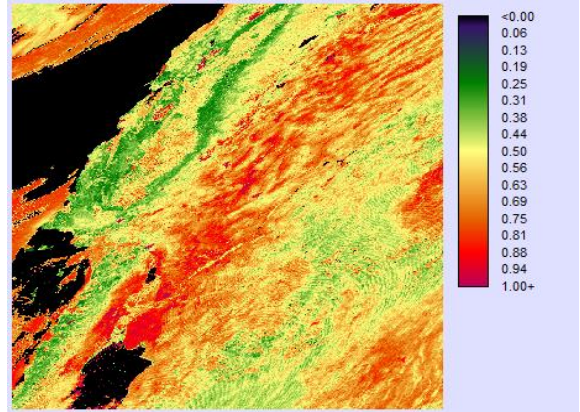
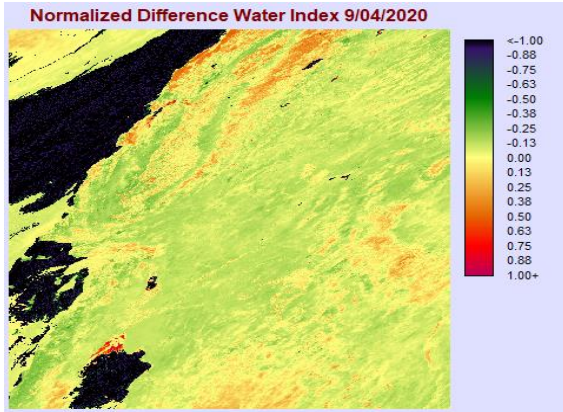
- Voiland, Adam. "Historic Fires Devastate the U.S. Pacific Coast." NASA Goddard Space Flight Center. 2020. <https://earthobservatory.nasa.gov/images/147277/historic-fires-devastate-the-us-pacific-coast>.
- Voiland, Adam. "Bobcat Fire Scorches Southern California." NASA Goddard Space Flight Center. 2020. <https://earthobservatory.nasa.gov/images/147324/bobcat-fire-scorches-southern-california>.
- Wang, L., Qu, J.J., 2007. NMDI: a normalized multi-band drought index for monitoring soil and vegetation moisture with satellite remote sensing. *Geophysical Research Letters*, 34, L20405, doi:10.1029/2007GL031021.
- Westerling AL, Cayan DR, Brown TJ, Hall B, Riddle LG. 2004. Climate, Santa Ana winds and autumn wildfires in Southern California. *EOS Trans Am Geophys Union* 85:289–300. <https://doi.org/10.1029/2004EO310001>
- Wu, Jianguo, Dennis E Jelinski, Matt Luck, and Paul T Tueller. 2000. "Multiscale Analysis of Landscape Heterogeneity: Scale Variance and Pattern Metrics." *Geographic information sciences* 6, no. 1: 6–19.
- Xu, H, F Abdul-Kadar, and P Gao. 2016. "An Information Model for Managing Multi-Dimensional Gridded Data in a GIS." *IOP conference series. Earth and environmental science* 34, no. 1: 12041–12047.
- Zhang, Shuhua, Xingong Li, and Jiangfeng She. 2020. "Error Assessment of Grid-based Terrain Shading Algorithms for Solar Radiation Modeling Over Complex Terrain." *Transactions in GIS* 24, no. 1: 230–252.
- Zhao, Hongkai. 2005. "A Fast Sweeping Method for Eikonal Equations." *Mathematics of computation* 74, no. 250: 603–627.

# Appendix: NMDI and NDWI Results









Appendix (Images 1-29). NMDI and NDWI Spatial-Temporal Results. Figure 17-29 shows Los Angeles County area.

